Building and Environment 247 (2024) 110916

Contents lists available at ScienceDirect

Building and Environment

journal homepage: www.elsevier.com/locate/buildenv

Can windcatcher's natural ventilation beat the chill? A view from heat loss and thermal discomfort

Miaomiao Liu [a], Salah Almazmumi [a,d], Pinlu Cao [b,*], Carlos Jimenez-bescos [c], John Kaiser Calautit [a]

[a] Department of Architecture and Built Environment, University of Nottingham, Nottingham NG7 2RD, UK
[b] College of Construction Engineering, Jilin University, Changchun, Jilin City, 130061, China
[c] School of Built and Natural Environment, University of Derby, UK
[d] Architectural Engineering Department, College of Engineering, Najran University, 66462, Najran, Saudi Arabia

ARTICLE INFO

Keywords:
Natural ventilation
Windcatcher
Field experiment
Cold climate
Heat loss
Thermal comfort

ABSTRACT

Windcatchers provide effective low-energy ventilation and summer passive cooling in temperate climates. However, their use in winter is limited due to significant ventilation heat loss and potential discomfort. Limited research has been conducted on quantifying windcatcher heat loss in cold climates, particularly through field studies. This study aims to evaluate the applicability of windcatchers in low-temperature conditions, with a focus on ventilation heat loss and thermal discomfort. Field experiments were conducted in Nottingham, UK, during an icy period. A 3D-printed prototype windcatcher and a test room were built and tested in such weather conditions. A Computational Fluid Dynamics (CFD) model validated against the field experimental data was employed to investigate the windcatcher's performance in a typical UK primary school classroom. The field experimental results indicate that the indoor airflow patterns are dynamic and continuously change with varying external wind conditions. Using static boundary conditions for ventilation analysis is inadequate, as it may lead to inaccurate predictions due to observed fluctuations and irregular airflow patterns. CFD modelling revealed significant over-ventilation in the classroom at external wind speeds of 3 m/s, despite being previously deemed as "satisfactory", "adequate", or "sufficient" ventilation. At wind speeds of 3 m/s or higher, the over-ventilation can cause a minimum 941.4 W heat loss, adding 4.7 kWh heating load and £1.6 electricity cost for a typical-sized single classroom during a 5-h occupied period. The research findings highlighted that control strategies should be introduced to reduce over-ventilation. Integrating heat recovery or thermal storage can enhance winter thermal conditions.

1. Introduction and literature review

Windcatchers, also known as wind towers, are traditional architectural elements used for passive cooling and ventilation in buildings [1]. Predominantly utilised in hot, arid regions like the Middle East and North Africa, windcatchers enable natural cooling without relying on mechanical systems [2]. Over the years, windcatchers have been combined with a range of techniques, such as solar chimneys, heat pipes, evaporative cooling, and earth-air heat exchanger (EAHE), to enhance their ventilation and cooling performance ([3–13]). While windcatchers have been extensively studied in hot climates, their adoption in cold/mild-cold regions like the UK has been limited. There have been several windcatcher installations, such as those at the Bluewater shopping centre [14] and the Queen's Building of DeMontfort University [15], but their widespread use is constrained. One reason is the limited operational period of windcatchers, especially in cold weather, which may cause significant heat loss and thermal discomfort (Fig. 1). To address this, recent studies ([16–20]) have integrated heat recovery devices like heat pipes, rotary thermal wheels, and fixed plate heat exchangers into windcatchers, which is expected to improve supply temperature and reduce ventilation heat loss.

However, these studies mainly discussed windcatchers' ventilation performance, heat recovery integrations, and air quality. There is a lack of in-depth analysis of heat loss and thermal discomfort caused by conventional windcatcher systems during cold conditions. Cold outdoor temperatures can lead to heat loss and increased electricity use during

* Corresponding author.
E-mail address: jlucpl@jlu.edu.cn (P. Cao).

https://doi.org/10.1016/j.buildenv.2023.110916
Received 16 August 2023; Received in revised form 8 October 2023; Accepted 9 October 2023
Available online 20 October 2023

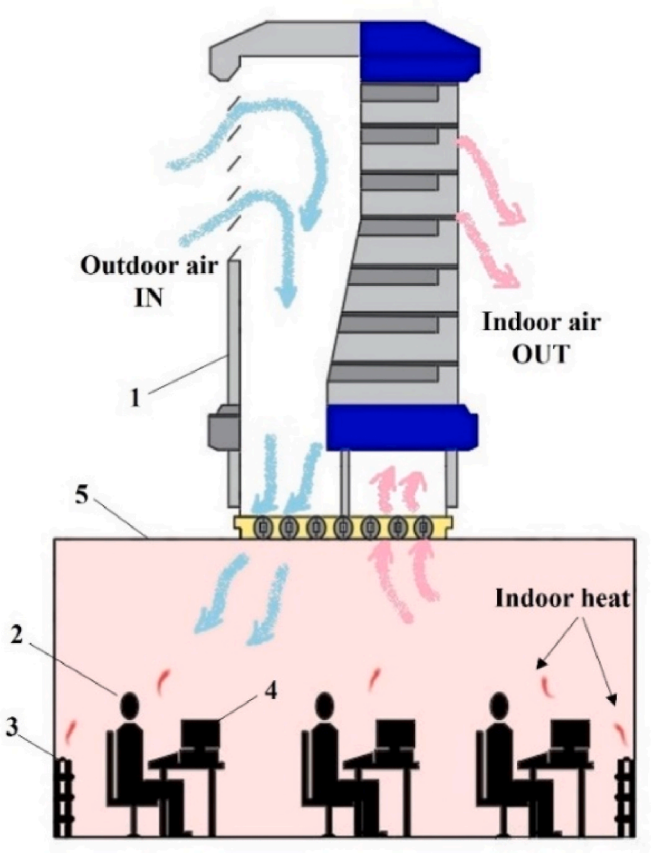

Fig. 1. A four-sided windcatcher's operation during cold climates. 1- windcatcher; 2- occupant; 3- heating elements; 4- computer; 5- ventilated space.

indoor-outdoor air exchange. Inadequate or excessive ventilation can cause thermal discomfort, affecting occupants' well-being and productivity. Cold climates exacerbate these issues due to temperature differences and drafts. This research gap is crucial for evaluating the cost-effectiveness of windcatchers and their energy-efficient management across various climates. Furthermore, most of the reviewed studies have mainly utilised CFD or wind tunnel testing, lacking field experiments. CFD and wind tunnel testing, while valuable for initial design assessments, may not accurately replicate real-world conditions. For example, many of the previous works ([10,11,13,19]) have modelled windcatchers in a wind tunnel-type domain. However, it did not capture the impact of the flat roof, which may cause flow separation and influence the windcatchers' performance. Real-world factors like terrain and wind patterns significantly affect windcatchers' performance. Windcatchers evaluated under static wind conditions can potentially lead to over- or under-conditioning in the occupied spaces. Field experiments can address site-specific factors that controlled environments usually cannot reproduce. Table 1 summarises the research topics in reviewed windcatcher studies.

This study established and tested a prototype windcatcher model and the test room at the University of Nottingham, UK, during the cold conditions. The influences of real-time outdoor temperatures, wind speeds, and wind directions on the airflow velocity and temperature features during the test periods were analysed. Following this, the transient responses of the windcatcher ventilation in terms of ventilation rate and heat loss were investigated. Moreover, a case study was conducted on a typical-sized UK primary school classroom using windcatcher ventilation to offer a broader view of windcatcher implementation in cold conditions. A validated CFD model against the field experimental data was employed to investigate the classroom's ventilation rate, thermal comfort, and ventilation heat loss across various wind speeds. The trade-offs between heat loss control, thermal comfort, and ventilation rate were analysed throughout this. The validation approach presented in this paper can also serve as a reference for other studies seeking to validate CFD simulations against field experimental data. These findings may guide more sustainable and efficient windcatcher designs, extending their function throughout the year. More efficient and advanced management/control mechanisms can be adopted in windcatchers to improve indoor comfort and minimise heat loss.

2. Field experiment method

The main objective of the field experiment is to obtain the real-time airflow velocity and temperature distributions in the windcatcher and test toom during the testing periods. Following the airflow data collection, the transient responses of the windcatcher and the test room regarding ventilation rate and ventilation heat loss were investigated.

2.1. Experimental site

The field experiments were conducted on open ground in the Jubilee campus, University of Nottingham, UK, located at 52.939°N and 1.197°W. As shown in Fig. 2, the test location is within a suburban built environment with a mix of residential areas, such as commercial establishments and recreational spaces, representing a typical residential area with roofs suitable for windcatcher installation. Understanding the

Table 1
Topics covered in the reviewed windcatcher studies.

Study	Ref	Methodology			Research topics			
		Numerical modelling	Lab experiment	Field experiment	Ventilation performance	Thermal comfort	Ventilation heat loss	Electricity savings
Foroozesh et al., 2022	[3]	✓				✓		
Abdallah, 2019	[4]			✓		✓		
Calautit et al., 2020	[6]	✓		✓	✓	✓		
Gilvaei et al., 2022	[7]	✓			✓	✓		✓
Jafari and Kalantar, 2022	[8]	✓			✓	✓		✓
Sadeghi and Kalantar, 2018	[9]	✓			✓			
Abdo et al., 2020	[10]		✓			✓		
Nejat et al., 2021	[11]	✓	✓		✓	✓		✓
Harrouz et al., 2021	[12]	✓				✓		✓
Sadeghi et al., 2020	[13]		✓			✓		✓
O'Connor et al., 2014	[16]		✓		✓			
Mahon et al., 2022	[19]	✓	✓		✓	✓		✓
Liu et al., 2022	[20]	✓			✓	✓		

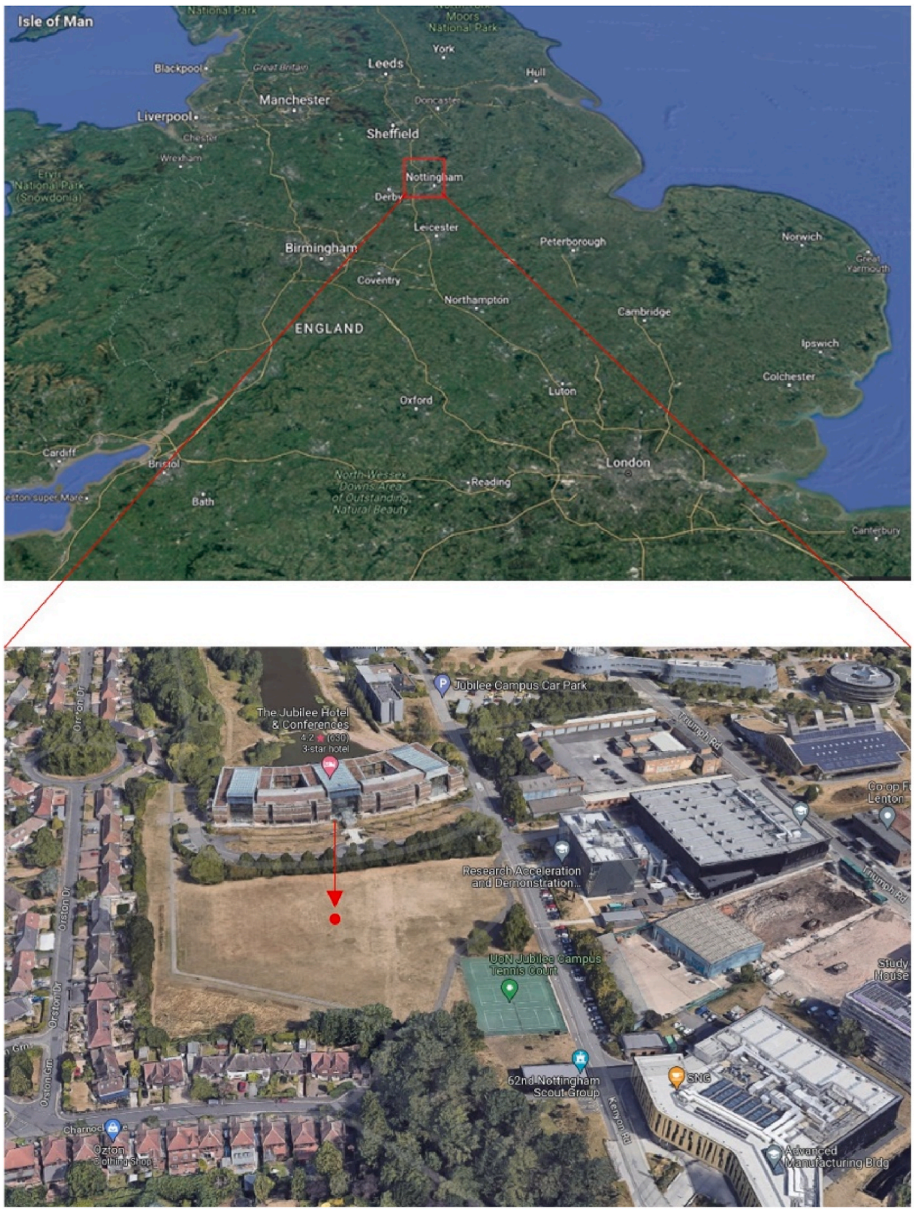

Fig. 2. The location of the experimental site in Jubilee Campus, Nottingham, UK.

performance of windcatchers in a suburban context allows for the transferability and scalability of the findings to similar settings.

Like most of the UK, Nottingham has a temperate oceanic climate (Köppen: Cfb) and experiences warm, mild summers and mild to cool winters throughout the year. The typical temperatures in Nottingham throughout the year are 2 °C in winter to 20 °C in summer. The monthly wind speeds range from 4.04 m/s to 5.53 m/s. The wind direction in Nottingham is predominantly from the southwest, west, or northwest due to the prevailing winds from the Atlantic Ocean. The field experiments were carried out in December, one of the UK's coldest months. During the test duration on December 16th from t = 15:10 to t = 16:30, the outdoor temperatures typically ranged from −0.6 °C to 0.9 °C.

2.2. Experimental prototype

Before commencing the fieldwork, the windcatcher and test room model were built, and the testing facility was set up. The windcatcher prototype ($W_w \times H_w \times L_w = 0.250\ m \times 0.250\ m \times 0.444\ m$) was 3D-printed using the material of Polylactic Acid (PLA). 3D-printed technology offers high accuracy in dimensions (±0.1 mm), especially for intricate and complex designs for the windcatcher like the louvres. It also offers a rapid and efficient method for prototyping, reducing the time and cost required for manufacturing. The windcatcher dimensions follow the previous works ([20,21]) with a 1:4 scale-down. The windcatcher consists of 7 layers of louvres set at a 45° angle ([20,21]). The dampers are not considered here because the windcatcher is assumed to be fully opened. The windcatcher is located on the roof of the test room ($W_r \times H_r \times L_r = 1\ m \times 1\ m \times 1.2\ m$). Detailed windcatcher dimensions are provided in the Appendix (Fig. A1). The test room, built with high-insulated polystyrene foam (50 mm thick), is fully closed and only ventilated by the windcatcher during the test time. Polystyrene foam has a low thermal conductivity, provides good thermal and moisture resistance, and reduces heat loss caused by infiltration and transmission through walls ([6,22]). Three tubular heating elements are evenly placed on the room floor, each with a diameter of 0.081 m, a length of 0.713 m, and a full power of 80 W. The distances between the heating elements are 0.250 m. The heating elements were switched on during the testing periods, representing the heat gained from radiators and

indoor occupants in real settings. Fig. 3 shows the windcatcher prototype and the test room.

2.3. Experimental setup and testing facility

Fig. 4 shows the experimental setup and the locations of the measurement points. A total of 5 Testo 405i hot-wire anemometer smart probes were used to measure the airflow velocity and temperature. These probes can measure velocities in the range of 0–30 m/s (0–2 m/s: ±0.1 m/s; 2–15 m/s: ±0.3 m/s) and temperatures from −20 °C to 60 °C (±0.5 °C). The data were wirelessly collected and stored in the Testo Smart App at an interval of 1 s. Four probes were positioned at the supply and exhaust planes at a height of 1.2 m above the room floor to measure the supply and exhaust air velocity. Additionally, one probe was placed outdoors to measure the wind speeds. The outdoor probe was positioned at the same height as the windcatcher's louvres and a horizontal distance of 5(H_r + H_w) from the test system. This arrangement was set up to obtain the incoming air velocity directly at the windcatcher's inlet.

In addition, a total of 8 type-K thermocouples were employed to measure the air temperatures, with 4 placed at the supply and exhaust plane (1.2 m above the room floor) and the other 4 indoors (0.6 m above the room floor). The temperature measurement accuracy is ±0.6 °C (50 °C) and ±0.5 °C (0 °C). All the thermocouples were connected to a data logger to collect the temperature data once a second. The data logger was connected to a laptop, and the real-time data were stored in the PicoLog software. A weather station of Ecowitt GW1100 was used to obtain the weather data, such as wind speed (0–5 m/s, ±1 m/s; ≥5 m/s, ±10%), wind direction, and air temperature (−40 °C–60 °C, ±1 °C). The weather data were wirelessly collected in the WSVIEW Plus App and then imported into Excel. The weather station should be located in an open area, away from obstructions that could block or disrupt the airflow. Considering the available heights of the tripod which holds the weather station and safety concerns, the installation height of the weather station was set at 2 m (within the generally recommended installation height range). The horizontal distance between the weather station and the test room was set at 5(H_w + H_r) to ensure that it was not affected by the airflow patterns around the test model. The measurement devices used are summarised in Table 2.

Section 2 provides an overview of the experimental site, surrounding context, wind conditions, and experimental setup. The dimensions of the prototype windcatcher model and the test room are detailed. The testing facility and the measurement points are introduced.

Fig. 3. The 3D-printed prototype of the windcatcher and the test room in the field test area.

3. CFD method

A typical-sized primary school classroom in the UK is selected as a case study to further investigate the effects of windcatcher ventilation during cold conditions. A validated CFD model is employed to evaluate the ventilation heat loss and indoor thermal comfort level. CFD simulation offers a cost-effective evaluation of the windcatcher's performance in different scenarios. The CFD modelling approach has previously been validated against wind tunnel testing, as can be found in Refs. [21,23]. Its validation against the field experimental data is detailed in Section 4.2.

3.1. CFD theory

The numerical model was developed using the ANSYS FLUENT (version 18.1) CFD program. The governing equations were described in Eqs. (1)–(3) [24]. They were solved under the following assumptions to simplify the modelling process. (1) The flow regimes inside the computational domain are considered fully turbulent; (2) The fluid domain is assumed to be steady and incompressible; (3) Radiation, infiltration and volumetric heat sources are not considered in this study; (4) The influences of air components such as moisture and CO_2 are not considered.

Continuity equation,

$$\frac{\partial \rho}{\partial t} + \nabla \cdot (\rho \vec{v}) = S_m \tag{1}$$

Where, ρ is air density; v is the fluid velocity; S_m is the mass added to the continuous phase from the dispersed second phase. Since only a single-phase flow is considered in this work, S_m is defined as 0.

Momentum equation,

$$\frac{\partial}{\partial t}(\rho \vec{v}) + \nabla \cdot (\rho \vec{v} \vec{v}) = -\nabla p + \nabla \cdot (\bar{\bar{\tau}}) + \rho \vec{g} + \vec{F} \tag{2}$$

Where, p is the static pressure; $\bar{\bar{\tau}}$ is the stress tensor; $\rho \vec{g}$ is the gravitational body force; $\vec{F}$ is the external body force, which is not modelled in this work.

Energy equation,

$$\frac{\partial}{\partial t}\left[\rho\left(e + \frac{v^2}{2}\right)\right] + \nabla \cdot \left[\rho v\left(h_f + \frac{v^2}{2}\right)\right] = \nabla \cdot \left(\kappa_{eff} \nabla T - \sum_j h_j \vec{J}_j + \tau_{eff} \cdot \vec{v}\right) + S_h \tag{3}$$

Where, e is the internal energy; h_f is the mass-specific enthalpy and only considers the dry air in this work; κ_{eff} is the effective thermal conductivity; T is the air temperature; h_j is the sensible heat of species j and $\vec{J}_j$ is the diffusion flux of species j, which are not modelled in the simulation work; τ_{eff} is the effective stress tensor; S_h includes the heat of chemical reaction, and any other volumetric heat sources that users have defined, which is not considered in this work.

The choice of the Renormalization Group (RNG) k-epsilon model for CFD modelling in this study is based on its proven accuracy in windcatcher ventilation studies ([25–28]) and its ability to balance accuracy and computational efficiency ([29,30]). The RNG k-epsilon turbulence model is primarily for simulating fully turbulent flows, typically at higher Reynolds numbers. The applicable y + range is 30–300 with standard wall functions. It should be noted that the RNG model may not yield precise results for low-velocity flows, such as those near walls, and it may face challenges when predicting complex flow phenomena like swirling or separated flows ([20,31]). In addition, it may have limitations when modelling buoyancy-driven flows characterised by significant temperature gradients [32]. The transport equations governing the RNG k-epsilon model are presented in Eqs. (4) and (5) [24].

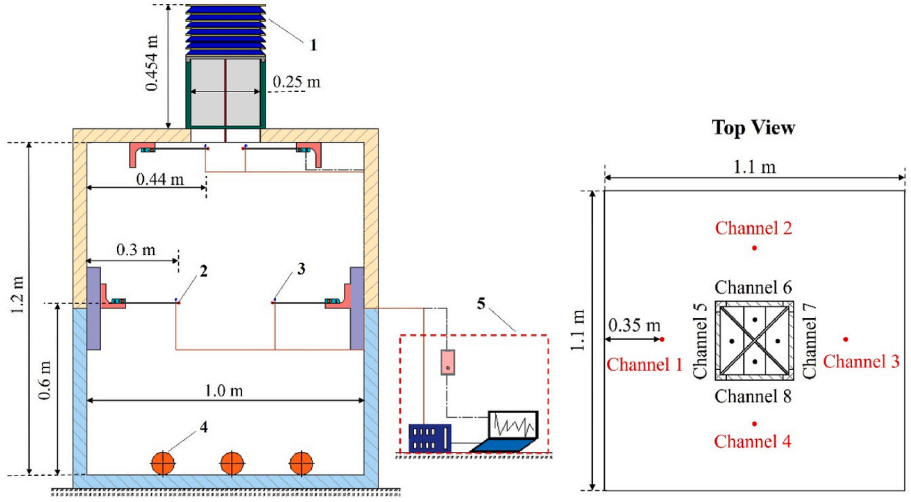

Fig. 4. The experimental setup of the windcatcher and the test room: 1-windcatcher; 2- hot-wire anemometer; 3- thermocouple; 4- tubular heating element; 5- data acquisition system.

Table 2
Summary of the measurement devices used during the field experiment.

Name	Model	Measurement ranges	Resolution	Accuracy	Data acquisition
Hot-wire anemometer	Testo 405i	Velocity: 0–30 m/s; temperature: 0–30 °C	Velocity: 0.01 m/s; temperature: 0.1 °C	Velocity: ±0.1 m/s at 0–2 m/s and ±0.3 m/s at 2–15 m/s; temperature: ±0.5 °C	Wirelessly connected to the Testo Smart Probe App; then to Excel
Weather Station	Ecowitt GW1100	Temperature range −40 °C- +60 °C; Wind speed range 0–50 m/s; wind direction 0°–360°	Temperature resolution 0.1 °C; velocity resolution 0.1 m/s; wind direction resolution 1°	Temperature accuracy ±1 °C; Wind speed accuracy ±1 m/s (speed <5 m/s) ±10% (speed ≥5 m/s)	Wirelessly connected to the WSVIEW PlusPlus App; then to Excel
Thermocouple Data Logger	Pico type-K USB TC-08	−270 °C- +1820 °C	0.025 °C	Sum of ±0.2% of reading and ±0.5 °C	Collected by data logger and PicoLog data logging software

$$\frac{\partial}{\partial t}(\rho k)+\frac{\partial}{\partial x_i}(\rho k v_i)=\frac{\partial}{\partial x_j}\left(\alpha_k \mu_{eff}\frac{\partial k}{\partial x_j}\right)+G_k+G_b-\rho\varepsilon-Y_M+S_k \quad (4)$$

$$\frac{\partial}{\partial t}(\rho \varepsilon)+\frac{\partial}{\partial x_i}(\rho \varepsilon v_i)=\frac{\partial}{\partial x_j}\left(\alpha_k \mu_{eff}\frac{\partial \varepsilon}{\partial x_j}\right)+C_{1\varepsilon}\frac{\varepsilon}{k}(G_k+C_{3\varepsilon}G_b)-C_{2\varepsilon}\rho\frac{\varepsilon^2}{k}+S_\varepsilon \quad (5)$$

Where k is the turbulence kinetic energy; ε is the dissipation rate; G_k represents the generation of turbulence kinetic energy due to the mean velocity gradients; G_b is the generation of turbulence kinetic energy due to the buoyancy; Y_M represents the contribution of the fluctuating dilatation in compressible turbulence to the overall dissipation rate, which is neglected in the modelling of incompressible flows; the quantities α_k and α_ε are the inverse effective Prandtl numbers for k and ε, respectively; S_k and S_ε are the user-defined source terms which are not considered.

3.2. Geometry model and computational domain

As mentioned in Jomehzadeh et al. [1], windcatcher ventilation is more suitable for high-density indoor spaces like classrooms. In the UK, there have been several windcatcher installations in educational buildings, such as Cranbrook Primary School in Ilford [33] and Tranent North Primary School in East Lothian [34]. The CFD geometry model utilises the dimensions representative of a typical-sized primary school classroom in the UK, thereby enabling the research findings to be more applicable to similar educational spaces.

As stated in Building Bulletin 103 (BB103) [35], junior classrooms designed to accommodate 30 pupils are recommended to possess an area of 55 m^2. Therefore, the classroom's dimensions are $W_c \times H_c \times L_c$ = 7.42 m × 7.42 m × 2.7 m [36]. The windcatcher's dimensions are $W_{cw} \times H_{cw} \times L_{cw}$ = 1.0 m × 1.0 m × 2.57 m, following the previous works ([20,21]). It should be noted that the windcatcher's height in the CFD model is over 4 times larger than the windcatcher's height used in the field experiments. This variation arises from the significance of the windcatcher's height in capturing wind and facilitating airflow. A taller windcatcher can efficiently capture higher-speed winds at increased heights and may enhance the vertical temperature gradient within the windcatcher through a natural stack effect. However, many previous studies have not mentioned the influence of windcatcher heights because these investigations evaluated the windcatchers' performance within controlled wind tunnel environments ([10,11,13,19]). This approach did not consider the impact of flow separation caused by the flat roofs, which may affect windcatchers' efficiency. For example, if a windcatcher is located within a flow separation zone, the effective wind speeds it captures will be reduced. Therefore, engineers or designers should consider windcatchers' sizes/locations and their surrounding context in real applications to maximise their efficiency. Overall, the dimensions of the windcatcher for the typical-sized classroom are $W_{cw} \times H_{cw} \times L_{cw}$ = 1.0 m × 1.0 m × 2.57 m.

It is generally recommended to set the fluid domain sizes as follows: 5H upstream and 15H downstream, with a lateral distance of 5H, where H represents the height of the tallest building model in the calculation area. This sizing configuration is commonly advised to minimise the impact of wind-blocking, flow recirculation, and local/global venturi effects [37]. However, a few studies have also proposed different domain sizes for airflow simulation around buildings. For example, according to Ref. [38], a downstream length of 3H is sufficient for the steady-state CFD simulation of a tall building. Therefore, before starting the simulation, we compared the effects of the computational domain

size on the simulation results, i.e., (1) LARGE: $W_{LE} \times L_{LE} \times H_{LE}$=(10$H_r$ + W_w) × (20H_r + L_w) × 6H and (2) SMALL: $W_{SL} \times L_{SL} \times H_{SL}$=(2$H_r$ + W_w) × (7H_r + L_w) × 4H. Fig. 5 shows the airflow velocity and temperature along the height from the air supply zone to the room floor (i.e., y = 0–5.0 m) with LARGE and SMALL domains. As the domain changed from SMALL to LARGE, the average airflow velocity and temperature differences were 5.1% and 1.7%, respectively. Considering the computational time duration, the SMALL domain was adopted in the following modelling, i.e., 3(H_w + H_r) for the upstream length, 3(H_w + H_r) for the lateral distances, and 8(H_w + H_r) for the downstream length.

3.3. Boundary conditions

In this CFD model, it is assumed that the 30 pupils and one male teacher are in sedentary activities, with metabolic rates of 1.0 met and 1.2 met, respectively [21]. According to Persily and de Jonge [39], 1 met is equal to a heat flux of 59.7 W/m^2 for a 32-kg male child aged 3–10 years, with a DuBois surface area of 1 m^2. For a 75-kg adult male aged 30–60 years with a DuBois surface area of 1.8 m^2, 1 met corresponds to a heat flux of 49.8 W/m^2. There are two heating elements inside the classroom, each with a heating power of 190 W [40]. It is assumed that the heat gains from the occupants and heating elements are fully converted to sensible heat, while the heating released from the lighting is not considered. As this research primarily focuses on the heat loss resulting from the windcatcher ventilation only, the thermal manikins and heating elements are not explicitly modelled. Instead, the internal heat gains obtained from the occupants and heating elements are assumed to be evenly distributed over the floor area of 7.42 × 7.42 m^2, resulting in a heat flux of 42 W/m^2. This modelling method can also be found in the simulation work of [20,41].

A uniform velocity inlet condition is implemented in the CFD model. The simplified treatment of the effects of the atmospheric boundary layer (ABL) flow, i.e., considering the influence of surrounding terrain features such as buildings and vegetation, was justified by the field test setup. The inlet velocity at the same height as the windcatcher's louvres was accurately captured by placing a velocity measurement point at the exact height of interest. Hence, the uniform inlet velocity boundary condition was deemed appropriate and justifiable for the CFD modelling.

The wind direction is pre-determined to be 0°. This choice is made because the windcatcher is multidirectional, and the impact of varying wind directions is not significant [42]. Additionally, buildings in regions with a prevailing wind direction typically opt for windcatchers that align with the dominant wind flow. Hence, the investigation of various wind directions is excluded. The outlet is set as atmospheric pressure. The mean outdoor temperature in December 2022 was 5 °C, as reported in Ref. [43]. The ground roughness height and constant are set as 10^{-6} and 0.5 m, respectively, representing a sandy region [20].

The fluid flow problem is solved by the steady-state Reynolds-averaged Navier-Stokes (RANS) equations. A pressure-based solver is employed to calculate the flow field. The gradient discretisation is performed utilising the "Least Squares Cell Based" method. A second upwind scheme is adopted for pressure-velocity coupling [44]. The top and side walls of the computational domain are symmetric boundaries. All walls are assumed to be non-slip. Solution convergence criteria are set at an energy residual of 10^{-6} and other residuals of 10^{-3} ([45,46]). Table 3 summarises the boundary conditions for the CFD model.

3.4. Sensitivity of the mesh configurations

Due to the intricate nature of the windcatcher model, particularly around the louvres with numerous small gaps, the fluid domain was discretised with unstructured meshes in the ANSYS Meshing tool. Curvature was applied to all surfaces. Smaller mesh control sizes were implemented for those small gaps to capture the airflow characteristics more accurately.

Before commencing the CFD simulation, a mesh-independence analysis was conducted to ensure that changes in mesh sizes did not affect the simulation results. Fig. 6a presents the variation in airflow velocity along the height from the air supply zone to the room floor (i.e., y = 0–5.0 m) for different mesh configurations: coarse (4,140,558), medium (7,472,287), and fine (13,396,255). A more consistent overall trend can be observed in the medium and fine mesh configurations compared to the coarse. As the mesh configuration changed from coarse to medium, the average air velocity decreased from 2.08 m/s to 1.88 m/s (11%). While as the mesh changed from medium to fine, the average air velocity increased from 1.88 m/s to 1.98 m/s (5%). Hence, the medium mesh configuration was selected in the CFD model. In the medium mesh configuration, the average y + value within the computational domain is 31, which aligns with the recommended y + range of 30–300 when employing the k-epsilon model with standard near-wall treatment. Fig. 6b shows the generated mesh of the fluid domain.

Table 3
The boundary conditions of the CFD model.

Parameters	Values
Inlet velocity	1–4 m/s
Wind direction	0°
Heat flux on the room floor	42 W/m^2
Outdoor temperature	5 °C
Outlet pressure	0 Pa atmospheric
Ground roughness height	10^{-6}
Ground roughness constant	0.5

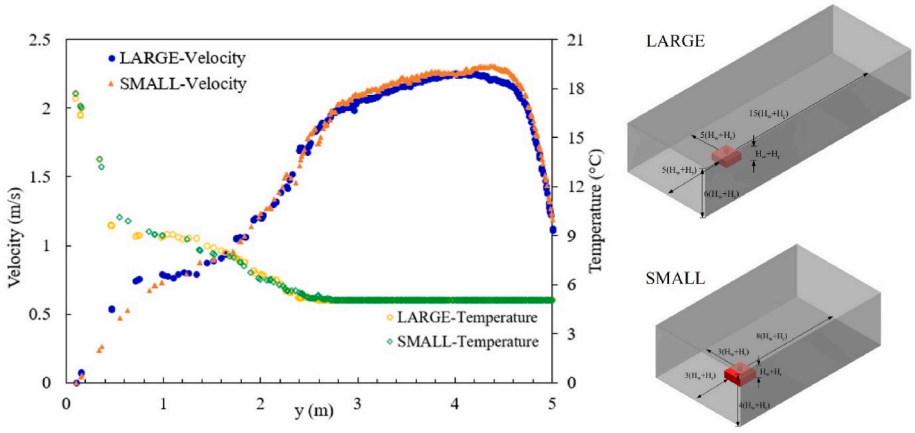

Fig. 5. The airflow velocity and temperature along the height from the air supply zone to the room floor (i.e., y = 0–5.0 m) with LARGE and SMALL domains.

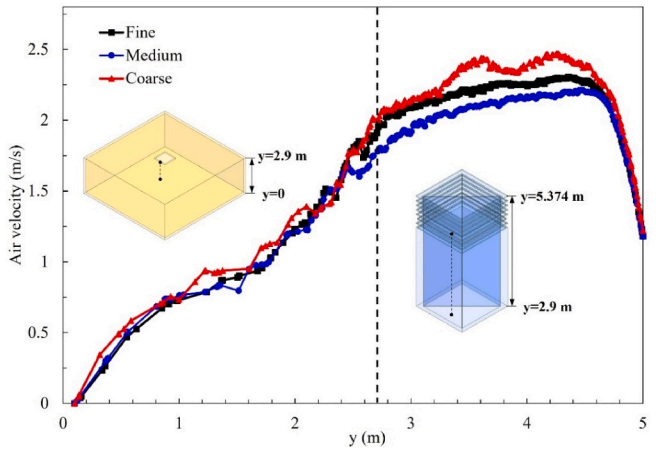

(a)

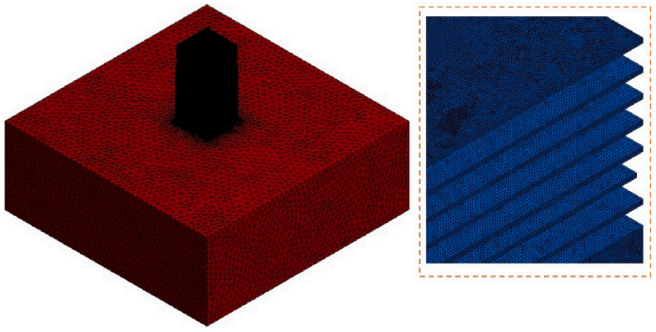

(b)

Fig. 6. (a) The mesh sensitivity analysis and (b) the schematic diagram of the surface mesh.

3.5. Critical parameters

A range of parameters, such as ventilation rate, nominal air changes per hour (ACH_n), ventilation heat loss, and mean age of air (MAA), were employed in this study, as calculated by Eqs. (6)–(10). The ventilation effectiveness at the breathing height was represented by air change effectiveness (ACE), as shown in Eq. (11).

Ventilation rate, denoted as q_s in m^3/s, represents the volume rate of outdoor air induced by the windcatcher into the occupied space per unit of time. q_s is calculated by Eq. (6) ([2,47]).

$$q_s = v_s \cdot A_{eff} \tag{6}$$

Where v_s is the airflow velocity entering the supply plane (m/s); A_{eff} is the effective supply quadrant cross-sectional area (m^2).

Nominal air changes per hour (ACH_n), denoted as N_n in 1/h, quantify how many times the air within the entire space is exchanged with fresh outdoor air in 1 h, as expressed in Eq. (7). A higher ACH_n indicates more frequent air turnover and better overall ventilation [42].

$$N_n = \frac{3600 \cdot q_s}{V} \tag{7}$$

Where V is the volume of the entire test room (m^3).

Ventilation heat loss, represented by Q in W, quantifies the amount of heat energy lost from the occupied space due to the windcatcher ventilation. Q is calculated by Eq. (8) ([48,49]).

$$Q = 0.33 \times N_n \times V \times (T_i - T_o) \tag{8}$$

Where 0.33 is the air heat capacity per cubic meter ($W \cdot h/m^3 \cdot K$); T_i and T_o are the indoor and outdoor temperature (K), respectively.

MAA refers to the average time for air to move from the point of supply to any given location in a ventilated space, which is expressed by Φ. A lower MAA indicates more frequent air changes and better ventilation [50]. MAA was calculated by introducing a user-defined scalar (UDS) into the transport model. To calculate the transport of an arbitrary scale Φ, one additional convection-diffusion equation was solved. For steady-state conditions, the equation takes the form in Eq. (9).

$$\nabla \cdot (\rho \vec{v} \Phi - \Gamma_\Phi \nabla \Phi) = S_\Phi \tag{9}$$

Where Φ is the scalar (MAA) to be solved; Γ_Φ is the diffusion coefficient of the scalar Φ; $S_\Phi = 1$ is the source term of the scalar Φ ([51,52]).

The diffusion coefficient of the scalar Φ is given by Eq. (10).

$$\Gamma_\Phi = \rho \cdot \left(2.88 \times 10^{-5}\right) + \frac{\mu_{eff}}{S_{c_t}} \tag{10}$$

Where the value of 2.88×10^{-5} in Eq. (10) means a constant laminar viscosity at the air temperature of 20 °C. Although the difference in laminar viscosity value reaches over 10% as the air temperature decreases to 0 °C, this variation is significant mainly in laminar flow areas, compared to turbulent flows. $S_{ct} = 0.7$ is the turbulent Schmidt number ([51,53]).

To assess ventilation effectiveness at the occupants' breathing height, air change effectiveness (ACE) is introduced. ACE, expressed as λ, is defined as the ratio between the nominal time constant and the MAA at the breathing height (Φ_{bh}), as shown in Eq. (11) ([42,54]). An ACE greater than or equal to 1.0 indicates perfect air mixing. ASHRAE 129 recommends a minimum ACE value of 0.95 at the breathing height for good mixing and ventilation effectiveness [55].

$$\lambda = \frac{\frac{V}{q_s}}{\Phi_{bh}} \tag{11}$$

Where Φ_{bh} is the MAA at the breathing height (s).

Section 3 describes the dimensions of the fluid domain. The CFD settings and mesh generation are discussed and justified. The critical parameters, such as ACH_n, MAA and ACE, are also described.

4. Results and discussion

Section 4 analyses the results of field experiments and CFD simulation and also presents the CFD model validation. Following the measurement of the temperature, velocity and wind direction in the field experiments, the transient responses of the windcatcher in terms of ventilation rate, ACH_n, and ventilation heat loss will be discussed. In addition, a detailed validation of the CFD model against the field experimental data is presented. The thermal comfort level, ventilation rate, ventilation heat loss, and potential additional heating energy demand in a typical-sized UK primary classroom are evaluated through the CFD modelling.

4.1. Field experiment results

The field experiments took place on Dec. 16, 2022, during the time t = 15:10-16:30. This specific period was characterised by low outdoor temperatures and low to moderate wind speeds. This allows us to evaluate the windcatcher's transient behaviour during a typical winter period in the UK when such ventilation systems are usually shut off. Fig. 7 shows the test location and the wind rose pattern during the testing period (t = 15:10-16:30). As can be seen, during the specific testing period, the wind speeds measured by the weather station ranged from 0.06 m/s to 1.04 m/s, with the wind directions mainly changing from NNW30° to NNE30°. Channel 5, facing north, served as the primary supply quadrant, while Channels 6 and 8 functioned as the secondary supply quadrants when the wind was not blowing directly from

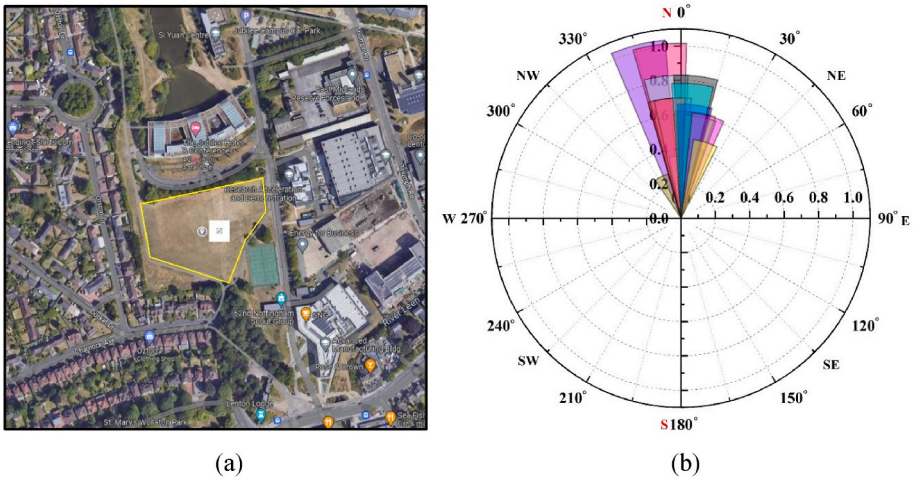

Fig. 7. The test location (a) and the wind rose pattern and (b) during the test periods from t = 15:10 to 16:30.

the north.

4.1.1. Time histories of the temperatures across channels 1-8

Unlike steady-state CFD modelling or controlled wind tunnel testing, the time histories of temperatures obtained from field experiments can directly depict windcatchers' transient behaviour and their interactions with the varying outdoor conditions. The real-time monitored data can aid in achieving more efficient control of windcatchers, thus reducing the additional heating energy demand arising from unnecessary ventilation during cold conditions.

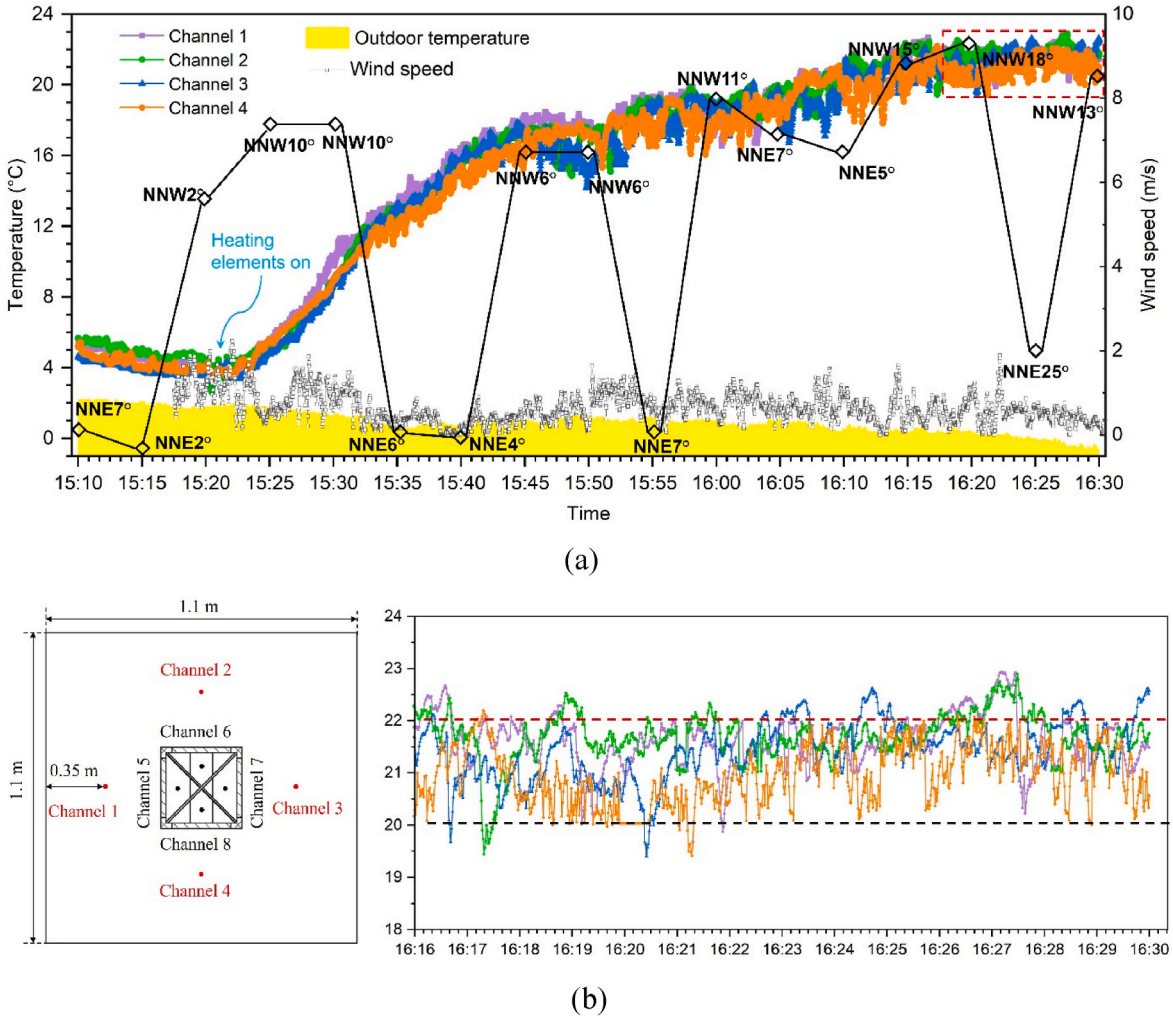

Fig. 8. (a) The indoor air temperatures measured at Channels 1–4 during t = 15:10-16:30 and (b) the zoom-in view of the indoor air temperatures measured at Channels 1–4 during t = 16:16-16:30.

Fig. 8a shows the indoor air temperatures measured at Channels 1–4 (indoor points) during t = 15:10-16:30. The overall trend observed was that the room temperature decreased as the outdoor temperature decreased before the heating elements were turned on (before t = 15:21). The outdoor temperatures were between 1.7 °C and 2.1 °C, while the indoor temperatures varied from 3.5 °C to 4.6 °C. Once the heating elements were turned on (after t = 15:21), the room temperature gradually increased until it reached a relatively stable state (t = 16:16-16:30). However, it should be noted that the temperature changing process demonstrates non-linearity, characterised by continuous fluctuations during both the decreasing, increasing and "stable" phases. Even during the "stable" state, the temperature readings in Channels 1–4 showed ongoing fluctuations within the range of 20–22 °C, as shown in Fig. 8b.

This finding contrasts with previous investigations ([11,18,23]) that utilised CFD modelling and wind tunnel testing, where the environmental variables, such as temperatures, are typically kept constant or assumed to vary linearly. However, such temperature data vary from second to second in the field experiments, which may be attributed to the changing wind conditions. Alternatively, these fluctuations could also stem from the air buoyancy effect and indoor thermal gradients. This observation is significant because, for example, fluctuations in temperatures should be considered when assessing potential discomfort periods for occupants. When conducting CFD or wind tunnel testing, it is important to perform deviation analysis or uncertainty propagation of the results, considering that the system is in a transient state rather than stable. Using fixed or static temperature profiles to evaluate thermal comfort or energy performance is inadequate and may result in inaccurate predictions as the fluctuations or irregular patterns have been observed in field experiments. From Fig. 8b, between approximately t = 16:16 and 16:30, the indoor temperatures reached a relatively "stable" condition, with values ranging between 20 °C and 22 °C. Hence, this period of temperature "stability" was the focus of the analysis.

Fig. 9 shows the temperatures measured at Channels 5–8 (supply and exhaust points) during two periods: t = 15:35-15:40 when the indoor temperatures in Channels 1–4 (indoor points) showed an increasing trend, and t = 16:16-16:30, during which the indoor temperatures in Channels 1–4 (indoor points) remained "stable". Large fluctuations can be observed during both periods, which differs from the steady-state indoor temperatures obtained in previous modelling work or laboratory experiments ([11,18]). The irregular patterns highlight the potential limitations of using constant boundary conditions when evaluating windcatchers' performance, as it may result in unnecessary ventilation or inadequate airflow. This inefficiency can cause energy waste and discomfort. In addition, windcatchers designed under fixed conditions may offer limited adaptability for buildings with diverse occupancy, usage aims and locations. This may also hinder their integrations with other building systems, such as shading or mechanical ventilation, which could respond to real-time conditions. Furthermore, windcatchers designed based on constant boundary conditions might not optimise natural airflow patterns or fully harness the potential benefits of varying wind conditions. It is essential to explore dynamic and responsive control strategies to enhance windcatchers' energy efficiency.

During t = 16:16-16:30, the temperatures recorded in Channel 5 were mostly at a lower level compared to the other three quadrants,

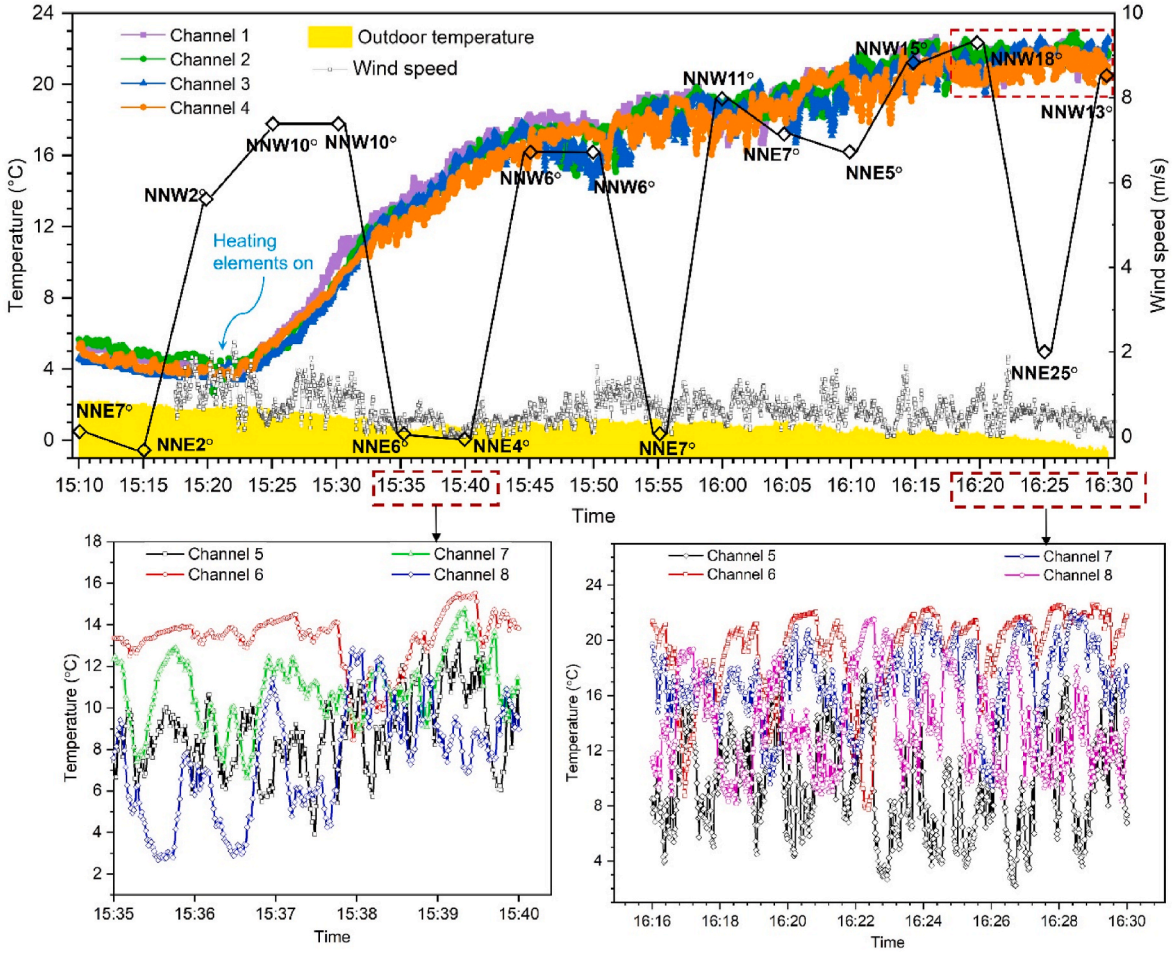

Fig. 9. The supply and exhaust air temperatures measured at Channels 5–8 during the test time t = 15:35-15:40 and t = 16:16-16:30.

around 4–8 °C. The temperatures in Channels 6 and 7 varied mainly between 16 and 22 °C, while temperatures in Channel 8 varied over a larger range, around 10–18 °C. For simplification, Channel 5 was considered the main air supply quadrant, which was also consistent with the wind direction recorded at the weather station (Fig. 7b). Channels 6 and 7 were identified as the primary exhaust quadrants. As the cold air supplied from Channel 5 enters the indoor space and encounters the warm indoor air, the warm air transfers its heat energy to the cold supply air through direct contact and mixing. In addition, the warm air exhausts through Channels 6 and 7 and carries away the indoor heat. It can also be noted that Channel 5 also experienced times when the temperatures reached 18–19 °C. This significant temperature change in Channel 5 may be attributed to rapid shifts in wind directions that can induce eddies and vortices. Additionally, it could arise from airflow disturbances caused by thermal plumes or gradients within the test room.

4.1.2. Time histories of the ventilation rate and ventilation heat loss in the test room

The following section analyses the ventilation rate and ventilation heat loss caused by windcatcher ventilation during the time t = 16:16-16:30, i.e., the indoor temperatures reached dynamic equilibrium. It can help identify opportunities to adjust ventilation settings and reduce electricity consumption by balancing ventilation rate and ventilation heat loss.

Fig. 10 shows the box plot of the ACH_n, wind speed and supply velocity at Channel 5 during the test time t = 16:16-16:30. ACH_n is calculated by Eq. (7) described in sub-section 3.5. As shown in Fig. 10, the 25%–75% of the wind speeds during t = 16:16-16:30 fell within the range of 0.36–0.68 m/s, and the corresponding supply velocities ranged from 0.13 to 0.44 m/s. The average wind speed was 0.54 m/s, while the average supply velocity monitored in Channel 5 was 0.32 m/s. This velocity distribution trend aligns with the velocity distribution patterns observed in the diffuse point within a benchmark four-sided windcatcher in Calautit et al. [56]. The ACH_n values ranged from 0.93 1/h to 82.97 1/h, with 25%–75% of the values varying from 5.63 1/h to 19.69 1/h. The mean ACH_n value during t = 16:16-16:30 was 11.25 1/h.

Moreover, ACE at the representative breathing height in the reduced-scaled test room was calculated to assess the ventilation effectiveness. According to Building Bulletin 101 (BB101), for a typical primary school classroom with a height of 2.7 m, the breathing level height is 1.1 m above the floor [57]. Since the test room is a reduced-scale model with a height of 1.2 m, the representative breathing height is 0.49 m above the room floor. Using data from the experiment, including wind directions, wind speeds, and outdoor temperatures during t = 16:16-16:30 (Δt_1 = 16:16-16:19, Δt_2 = 16:20-16:24, and Δt_3 = 16:25-16:29), ACE at the representative breathing height was calculated through CFD, as shown in Fig. A.2. As can be seen, the average ACE values during the time periods ranged from 1.12 to 1.15, all of which were higher than 1.0. This indicates that during t = 16:16-16:30, the air at the representative breathing height was well-mixed, and the windcatcher can effectively deliver fresh outdoor air indoors.

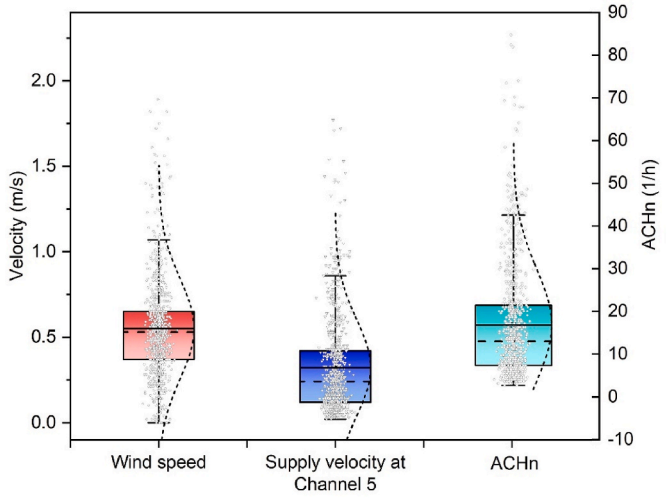

Fig. 10. The box plot of the wind speed, supply velocity at Channel 5 and ACH_n during the test time t = 16:16-16:30.

Fig. 11 shows the ventilation heat loss, ventilation rate, wind speed, and outdoor temperature during the test time t = 16:16-16:30. As can be seen, the wind speeds during the testing period fluctuated around 0.10–1.25 m/s, and the outdoor temperatures were mainly between −0.6 °C and 0.9 °C. Ventilation rates in Channel 5 mostly ranged from 0.78 L/s/m^2 to 15.47 L/s/m^2. Several ventilation rates also reached 16.41 L/s/m^2 to 27.66 L/s/m^2, with the corresponding supply air velocities recorded at high levels, i.e., from 1.05 m/s to 1.77 m/s. Similarly, the ventilation heat loss also showed an increasing trend with the increased ventilation rate, from 47.2 W at a ventilation rate of 1.88 L/s/m^2 to 380.1 W at 15.16 L/s/m^2. At the peak supply velocity, the ventilation rate reached the highest value of 27.66 L/s/m^2 and the heat loss was 696.53 W. It can be observed that the ventilation rate can reach 2.50 L/s/m^2 at the average wind speed of 0.60 m/s. A ventilation heat loss of 63.27 W can be caused if there is a temperature difference of 22 °C (comfortable level) between the indoor and outdoor environments and a ventilation rate of 2.50 L/s/m^2. From this point of view, conventional windcatcher ventilation might not be suitable for cold conditions. If they are to be utilised in such environments, windcatchers should be accompanied by control strategies that enable airflow adjustment into the room. Alternatively, they can be combined with preheating air units or heat recovery units to improve the supply air temperature.

4.2. Validation of the CFD model

Before commencing the simulation work, it is important to validate the CFD model to ensure its reliability. This section aims to analyse and compare the supply velocity and temperature obtained from the CFD model with that acquired from the field experiments.

Fig. 12 shows the plot of the supply velocity obtained at Channel 5 in the field experiments during the testing period of t = 15:10-16:30 and the corresponding supply velocity in the CFD model. To reduce the limitation that the weather station can only record the weather data every 5 min while the wind directions varied at each second, we simulated the supply velocities for two scenarios using the CFD model: one with a wind direction of 0° (representing perpendicular wind entry into Channel 5) and the other with a wind direction of 60°. In addition, as mentioned in the previous simplification, this study focuses on airflow patterns in the main air supply quadrant (Channel 5), despite the potential existence of two supply quadrants.

Given the difficulties of individually matching each data point to its corresponding simulated value, considering the variability of wind directions and a large amount of data, this study adopted a different validation strategy. First, all the supply velocity values measured at Channel 5 during the field experiments and the corresponding wind speeds were plotted. Subsequently, the numerical supply velocities under the 0° and 60° wind directions were obtained from the CFD model. Finally, the experimental and simulated results were compared and analysed.

As shown in Fig. 12, the supply velocity in both the CFD simulation and field experiment is in line and within the same range. From the simulation results, the supply velocity was 1.08 m/s and 0.44 m/s when the wind angle was 0° (represented by LINE0) and 60° (represented by LINE60), respectively, at a wind speed of 2 m/s. From the experimental data, the wind speeds mainly ranged from 0 to 1.2 m/s. It can also be observed that there are some points where the supply air velocity exceeds the outdoor wind speeds. This might be attributed to measurement errors caused by rapid shifts in the wind patterns. Such points with

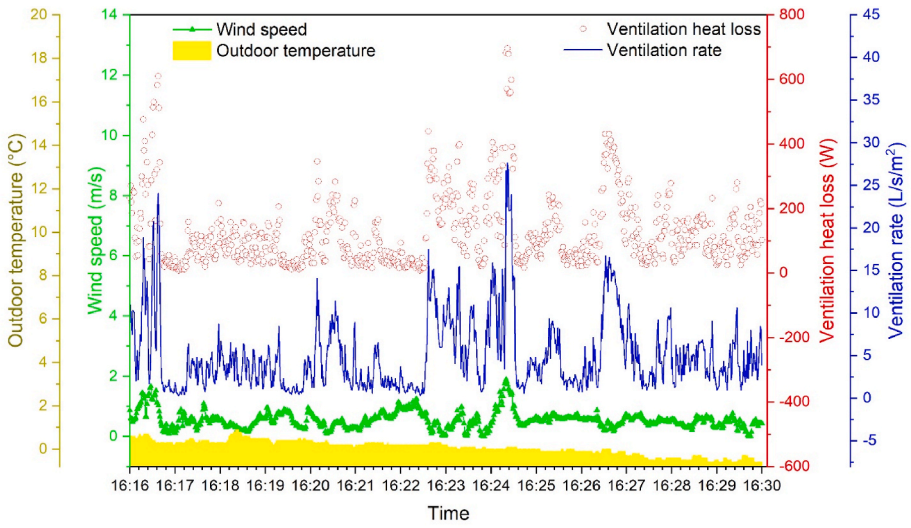

Fig. 11. The ventilation heat loss and ventilation rate against the wind speed and temperature during the test time t = 16:16-16:30.

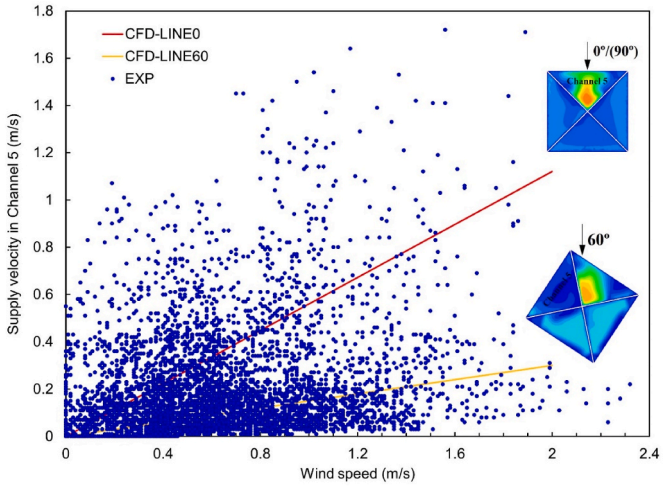

Fig. 12. The comparison of the supply velocity at Channel 5 between the CFD and the field experiments.

measurement errors contribute a small portion of the experimental data and have been excluded from the analysis. Overall, the plotted experimental supply velocity values are mainly distributed between LINE 0 and LINE 60. Specifically, there is a trend where a significant portion of the experimental data aligns with and is concentrated around LINE 60.

The discussion of Fig. 12 also supports the point that relying solely on CFD for studying ventilation rates is insufficient, as CFD mainly assists in understanding the overall trend. However, since CFD cannot fully replicate the complex and varying boundary conditions observed in experiments, discrepancies can arise between simulation results and experimental data. Windcatcher field experiments can capture transient behaviours that are challenging to reproduce in CFD simulations, especially when dealing with unsteady flows or complex geometries.

In addition to verifying the supply velocity, we also simulated the average supply temperatures within four 60-s periods, i.e., t = 16:17 (Δt = 16:17:00-16:17:60), t = 16:19 (Δt = 16:19:00-16:19:60), t = 16:23 (Δt = 16:23:00-16:23:60), and t = 16:28 (Δt = 16:28:00-16:28:60), respectively. We then compared these simulated values with the experimental data, as illustrated in Fig. 13a. It can be found that the CFD model underestimated the supply temperatures compared to the field experimental data. However, a consistent trend between the CFD and experimental data can still be observed.

Fig. 13b displays the average indoor (Channels1-4) and exhaust (Channels 6–7) temperatures measured in the field experiments at t = 16:17, 16:19, 16:23, and 16:28. As can be observed, during t = 16:17 and 16:19, the exhaust temperatures were lower than the indoor temperatures, measuring 5.32 and 5.78 °C, respectively. This observation suggests a potential air short circuit (ASC), i.e., cold supply air bypasses the ventilated space and directly exits through the exhaust quadrants. Such a phenomenon could impact the accuracy of temperature measurements in the experiments.

To gain deeper insights into this disparity, Fig. 13c visualises the velocity vectors near the supply and exhaust quadrants in the CFD model, taking t = 16:19 as an example. While it is impractical to visually observe airflow characteristics on a specific plane during experiments, CFD allows for a more cost-effective observation of this phenomenon. As can be seen, some of the warm exhaust air re-enters the supply quadrant, leading to air disturbance. This observation aligns with the numerical findings of Nejat et al. [58], who identified the presence of ASC and air disturbances among the supply and exhaust quadrants. These air disturbances could also contribute to the significant difference between the experimental supply temperatures and the CFD values.

The potential ASC or air disturbances may cause inefficient ventilation, resulting in poor air quality and discomfort for occupants. Fig. 14a shows the MAA distribution in the cross-sectional plane at t = 16:19. The MAA distribution basically followed the airflow pattern in windcatcher ventilation. It reached its lowest value of 6 s in the supply jet and then increased to 213 s in the recirculation zone where airflow became stagnant. Near the room ceiling, the MAA values were higher, reaching 224 s. Following the overall distribution of MAA in the test room, Fig. 14b shows the distribution of ACE with streamlines in the representative breathing height at t = 16:19. It can be observed that at the centre of the breathing plane, the ACE value peaked at 1.75, indicating efficient air mixing in this region. Along the dominant wind direction, near-wall areas showed ACE values ranging from 1.02 to 1.15. Stagnant zones where the airflow velocity was low were observed, resulting in ACE values around 0.88–0.97. According to ASHRAE 129, an ACE greater than 0.95 is recommended for achieving good mixing and ventilation effectiveness [55]. Although the average ACE at the representative breathing height was 1.03, areas affected by ASC may experience stagnant air and poor ventilation.

To minimise the possible influence of the air disturbance, we further plotted the supply temperatures at several test time points (t = 16:16:23, 16:17:48, 16:19:05, 16:24:31 and 16:26:43) obtained from the field experiments. These supply temperatures were then compared to the

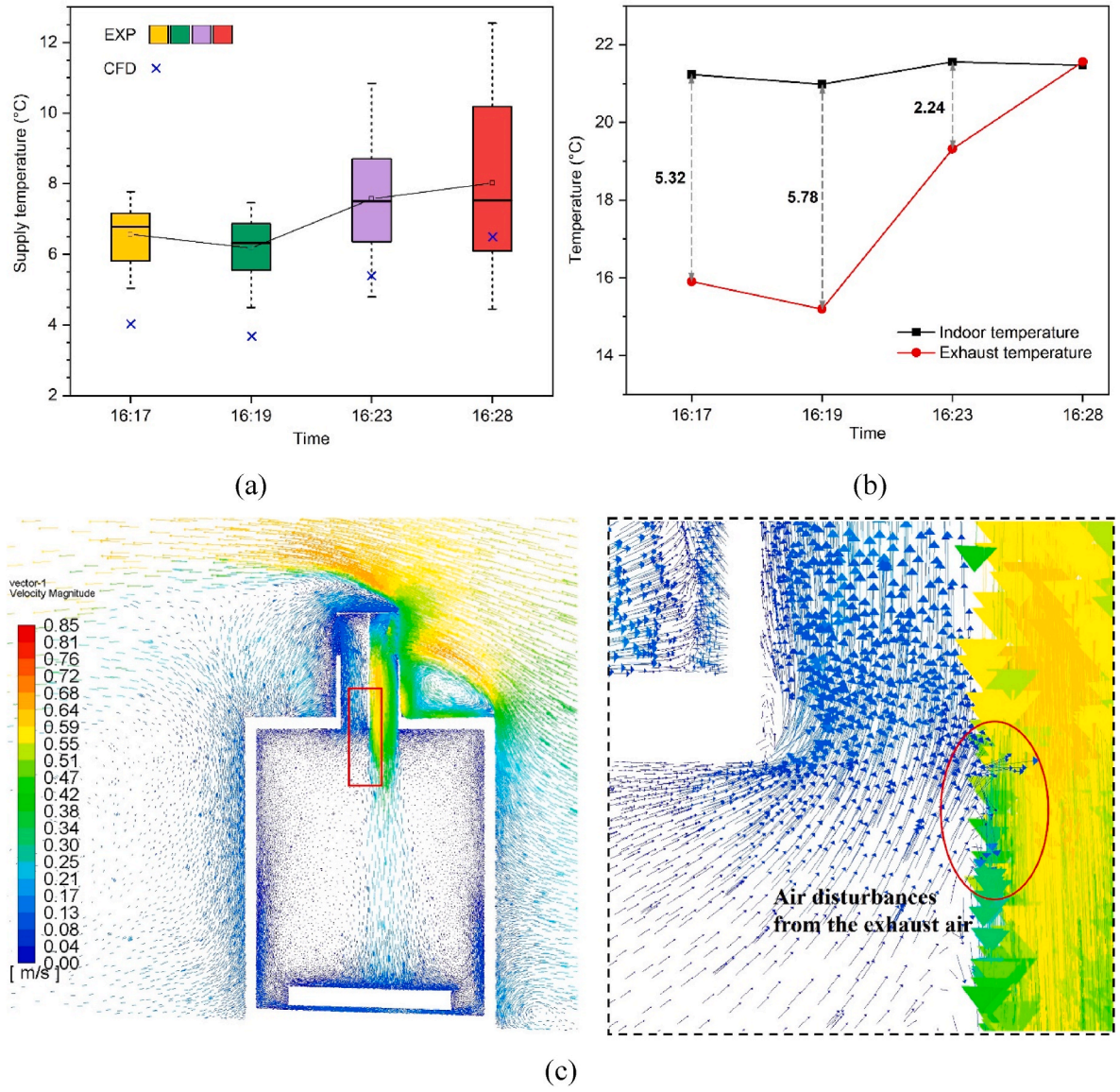

Fig. 13. (a) The comparison of supply temperatures between the CFD and field experiments at t = 16:17, 16:19, 16:23 and 16:28; (b) the plot of the indoor and exhaust temperatures obtained from the field experiments at t = 16:17, 16:19, 16:23 and 16:28; (c) the velocity vectors near the supply and exhaust quadrants at t = 16:19.

numerical results obtained from the steady-state CFD model, as shown in Fig. 15. Table 4 summarises the wind conditions recorded in the experiment at these time points. The selection of these points is because these supply temperatures are probably less influenced by the air disturbances from the exhaust air. In addition, to ensure a more accurate input of the velocity boundary conditions in the CFD model, the points with wind speeds lower than 0.1 m/s were excluded. As can be seen from Fig. 15, the CFD and experimental results show a more consistent trend, while the CFD model underestimated the supply temperatures at these time points. The average error between the CFD and experimental values across the time points is 17%.

Section 4.2 shows the CFD model validation against the field experimental data. Overall, the CFD results show a similar trend to the experimental data, but the values, such as the supply temperatures, are generally lower than the experimental values. An average error of 17% can be obtained between the CFD and experimental values across several time points, as shown in Fig. 15. This disparity becomes more pronounced when averaging over each 60-s interval within each time point, as shown in Fig. 13a. These differences could potentially be attributed to factors such as the experimental measurements being affected by the warm exhaust airflow, leading to higher recorded values for supply temperatures. Alternatively, these disparities might arise from the CFD's limitations in fully replicating the boundary conditions of the field experiments, resulting in inaccuracies in the simulation results.

4.3. *Case study: thermal comfort level and ventilation heat loss in a typical-sized classroom*

The following section will evaluate the ventilation rate and heat loss in a typical-sized classroom at a range of wind speeds using the validated CFD model. The thermal comfort level in the classroom will also be discussed.

4.3.1. *Ventilation heat loss*

Fig. 16 illustrates the relationship between the wind speeds and the ventilation heat loss in a typical-sized primary school classroom at the outdoor temperature of 5 °C and wind direction of 0°. The findings indicate that as the wind speed increases, the ventilation rate and

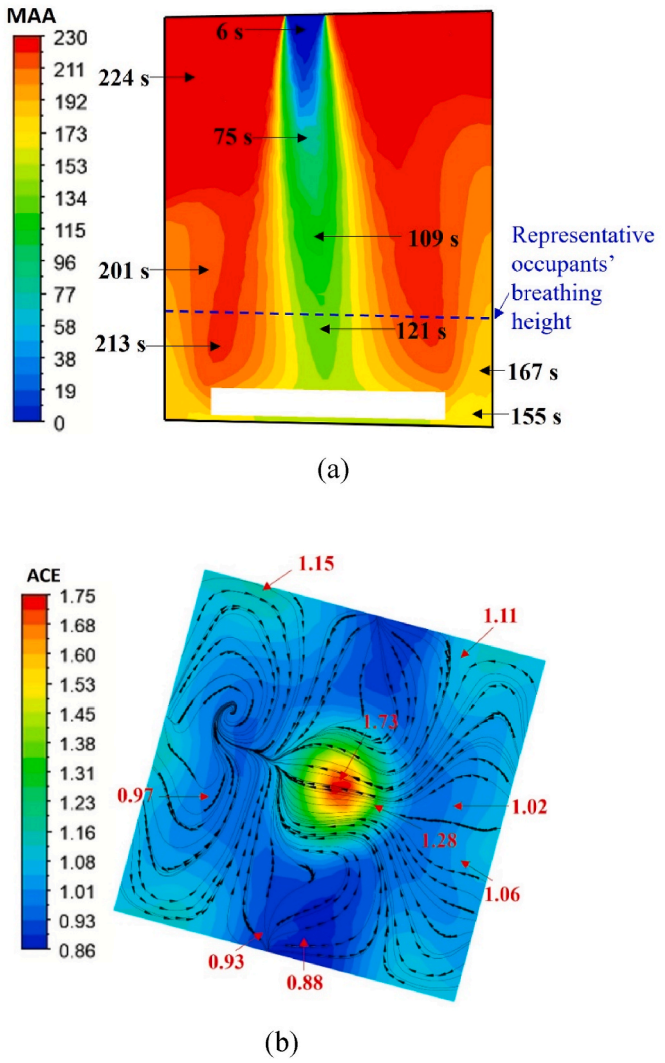

Fig. 14. The visualisation of MAA at the cross-sectional plane (a) and ACE and streamlines at the representative breathing height (b) at t = 16:19.

ventilation heat loss show an increasing trend. This aligns with the observations in the field experiments. As can be seen, when the wind speed is 1 m/s, for a classroom occupying 31 people, the ventilation rate is 4.27 L/s/person or 2.41 L/s/m^2. The corresponding ventilation heat loss is 2479.2 W. As the wind speed increases to 2 m/s, the ventilation rate increases to 8.39 L/s/person or 2.41 L/s/m^2.

According to BB101 guidelines 2018, a teaching space accommodating 30 students and one or two staff members should maintain a minimum ventilation rate of 2.3 L/s/m^2 or 8 L/s/person for the entire room [57]. Therefore, the ventilation rate can meet the recommended requirements when the external wind speed reaches 2 m/s. In regions where the average wind speed is greater than 2 m/s, prevailing wind conditions may potentially result in spaces being over-ventilated. Given that the UK's average wind speed falls within this range [59], it becomes crucial to consider control strategies, such as adjustable louvres/dampers, for most windcatcher installations. As the wind speed continues to increase to 4 m/s, the ventilation rate reaches 17.02 L/s per person or 9.58 L/s/m^2, resulting in a heat loss of 2838 W. At a wind speed of 4 m/s, a much higher ventilation rate than required is achieved, which could lead to over-ventilation of the occupied space and significant ventilation heat loss. While the overall ventilation rates are significantly high, it is important to evaluate the ventilation effectiveness at the breathing heights in real-world applications, as some areas may encounter issues such as stagnant air and insufficient air mixing.

From the above discussion, it can be seen that for the typical-sized primary school classroom ($W_c \times H_c \times L_c = 7.42 \times 7.42 \times 2.7$ m^3), the supply air rate provided by the windcatcher ($W_{cw} \times H_{cw} \times L_{cw} = 1 \times 1 \times 2.57$ m^3) can meet the ventilation requirements in BB101 at a wind speed of 2 m/s. Figs. A.3 and A.4 also present the velocity and temperature distributions in the windcatcher and classroom at a wind speed of 2 m/s and outdoor temperature of 5 °C. From Fig. A.3b, the average supply velocity is 0.98 m/s, and the exhaust velocity is 0.39 m/s. This indicates that windcatcher ventilation can efficiently replace indoor air with outdoor air. As depicted in Fig. A.4, when the cold supply air is introduced into the classroom through the windcatcher and mixes with the indoor warm air, the warm indoor air exhausts (12.5 °C) through other openings of the windcatcher. This observation implies that indoor heat has been lost through the exhaust quadrants, resulting in ventilation heat loss.

At a wind speed of 3 m/s, the windcatcher ventilation results in a heat loss of 2779.9 W, wherein the excessive ventilation leads to a heat loss of 941.4 W. This indicates that over 5 h, an additional heating load caused by over-ventilation could reach 4.7 kWh for the single classroom. According to the Department for Business, Energy & Industrial Strategy (BEIS), UK, the average electricity price between October 1, 2022 and July 1, 2023 was £0.34/kWh [60]. Therefore, the extra electricity cost due to the over-ventilation for the single classroom during 5 occupied hours would amount to £1.6.

4.3.2. *Thermal comfort level*

In addition to predicting the heat loss values, the thermal comfort level in the room is also quantified based on a psychrometric chart (represented by the Givoni bioclimatic chart). The Givoni bioclimatic chart is primarily designed for residential-scale buildings and is based on anticipated indoor temperatures ([61,62]). It delineates comfort boundaries and identifies heating/cooling or dehumidification/humidification strategies necessary for different zones [63]. Additionally, we incorporated the average responses of occupants on a seven-point heat-sensitivity scale, known as predicted mean vote (PMV). The background colour gradient, blue to red, represents the votes from cold to hot, respectively, encompassing the categories of cold, cool, slightly cool, neutral, slightly warm, warm, and hot [64]. The PMV classification employed in this study adheres to the EN 15251 standard released by the European Committee for Standardisation for buildings without mechanical heating/cooling systems [65]. PMV is influenced by factors such as occupants' activity level, air velocity, and clothing insulation level. The clothing insulation level for primary school students aged 9–11 years old was suggested to be 0.97–0.98 clo [66], and the metabolic rate was assumed to be 1.0 met since sedentary activities are probably the most common scenarios in classrooms [21].

Fig. 17a shows the effects of different wind speeds on indoor thermal comfort in a typical-sized primary school classroom. The mean temperature and relative humidity in December 2022 were 5 °C and 90%, respectively [43]. It can be observed that when the wind speeds are between 2 and 4 m/s, the average room temperatures fall outside the thermal comfort zone. At a wind speed of 1 m/s, the room temperature can achieve a comfortable level. Nonetheless, considering the relative humidity is 90%, dehumidification should be considered to attain a comfortable indoor environment. It can be predicted that wind speeds below 1 m/s may lead to overheating in the classroom. Based on the PMV results, occupants may feel neutral when the outside wind speed is 1 m/s, and slightly cool to cool when the outside wind speed increases from 2 m/s to 4 m/s.

Fig. 17b shows the temperature distribution contours for the middle horizontal plane (y = 1.45 m) and the supply and exhaust plane (y = 2.8 m) within the classroom at different wind speeds. As can be seen, the average room temperature gradually increases as the wind speed decreases from 4 m/s to 1 m/s, with the temperature difference between the supply and exhaust quadrants reaching 17 °C at the wind speed of 1 m/s. This means that a large amount of indoor heat has been wasted

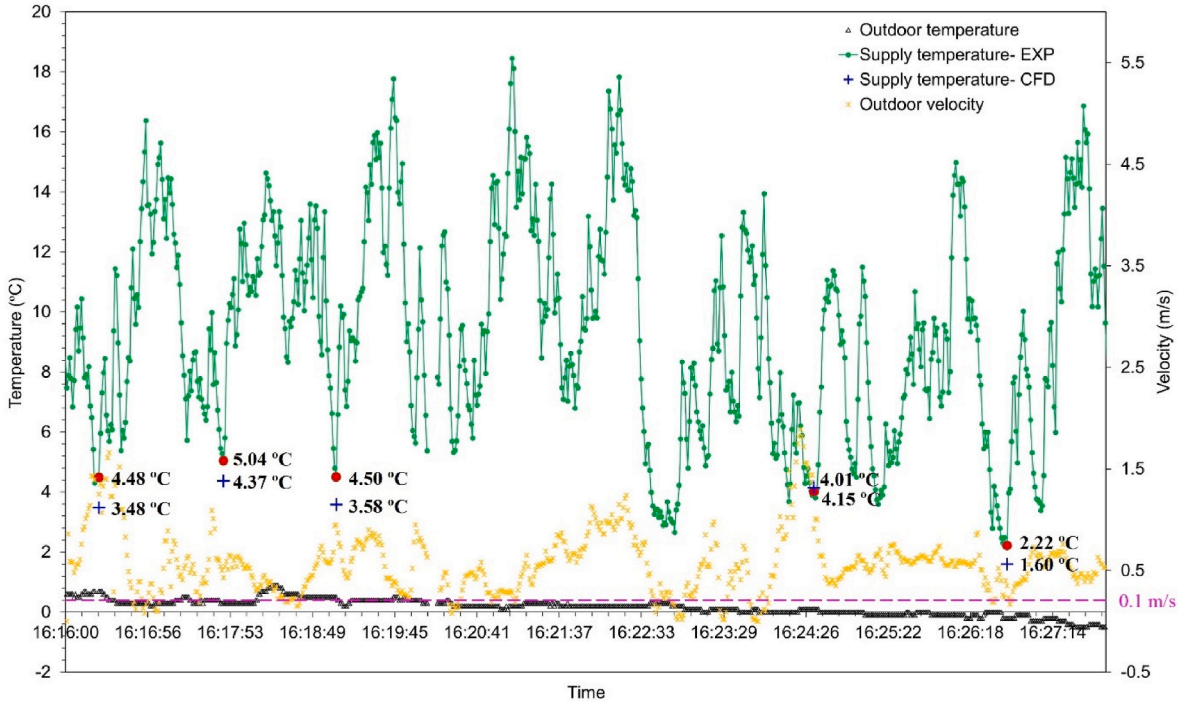

Fig. 15. The supply temperature obtained at Channel 5 in the CFD and experiment at the time points of t = 16:16:23, 16:17:48, 16:19:05, 16:24:31 and 16:26:43.

Table 4
The outdoor temperature, wind speed and wind angle at the time points of t = 16:16:23, 16:17:48, 16:19:05, 16:24:31 and 16:26:43.

Time	16:16:23	16:17:48	16:19:05	16:24:31	16:26:43
Wind speed (m/s)	1.07	0.59	0.77	1.00	0.17
Wind angle	NNW15°	NNW15°	NNW18°	NNE25°	NNE25°
Outdoor temperature (°C)	0.7	0.3	0.5	0.1	−0.2

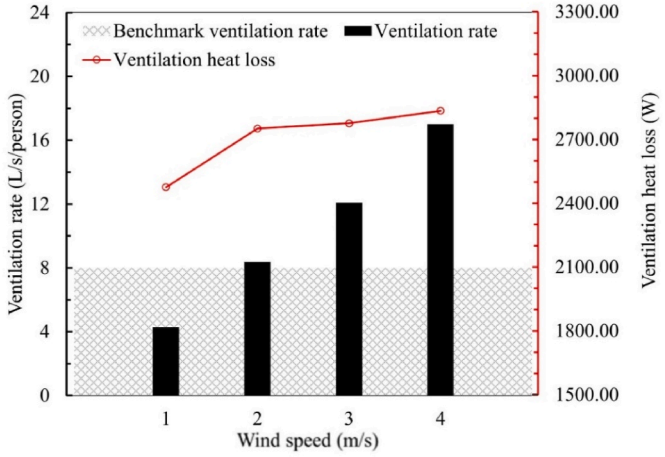

Fig. 16. The ventilation rate and heat loss at wind speeds of 1–4 m/s.

under these conditions. Heat recovery units or thermal energy storage systems can be introduced for windcatchers to collect the waste heat to preheat the incoming air ([19,20,67]).

5. Significance and limitations of this work

Windcatchers offer energy-efficient ventilation, but poor management can lead to heat loss and discomfort in cold conditions. In this study, we conducted field experiments in Nottingham during December, a cold month in the UK, to analyse the ventilation rate and heat loss. A validated CFD model against the field experimental data was also presented. The experimental findings indicate that temperature and velocity profiles exhibit non-linear variations, suggesting that previous works using fixed or predefined constant airflow data may yield deviations or inaccurate results when evaluating windcatchers' performance. The field experimental data can be utilised as an input for building energy simulations to enable more efficient control of ventilation systems, minimising unnecessary heating energy loads and effectively managing indoor conditions. In addition, the study provides a methodology for validating the CFD model using field experimental data.

While the field experiments provided valuable insights, it is crucial to recognise that they were conducted over a brief period, constrained by the limited operational duration of the heating elements. To improve the accuracy and reliability of future studies, more frequent recording of weather conditions is recommended. In our case, the weather station logged data every 5 minutes, but shorter intervals could capture more dynamic environmental changes. Furthermore, it is important to note that the test room used in this study is a hypothetical model, and we did not delve into potential heat loss caused by building operations or designs. This is a critical consideration for real-world applications. Regarding the CFD validation, the RNG model may not accurately simulate buoyancy-driven effects and flows with low velocities. Challenges remain in achieving a comprehensive validation of the CFD model. For instance, the dynamic nature of the external wind flow presents difficulties in integrating real-time boundary conditions into the CFD simulation.

6. Conclusion and future work

This study presents a field investigation of the effects of a prototype windcatcher ($W_w \times H_w \times L_w = 0.250\ m \times 0.250\ m \times 0.444\ m$) on the test room ($W_r \times H_r \times L_r = 1\ m \times 1\ m \times 1.2\ m$) during low-temperature conditions. The experiment was conducted at Jubilee Campus, University of Nottingham, UK on December 16, 2022, with wind speeds

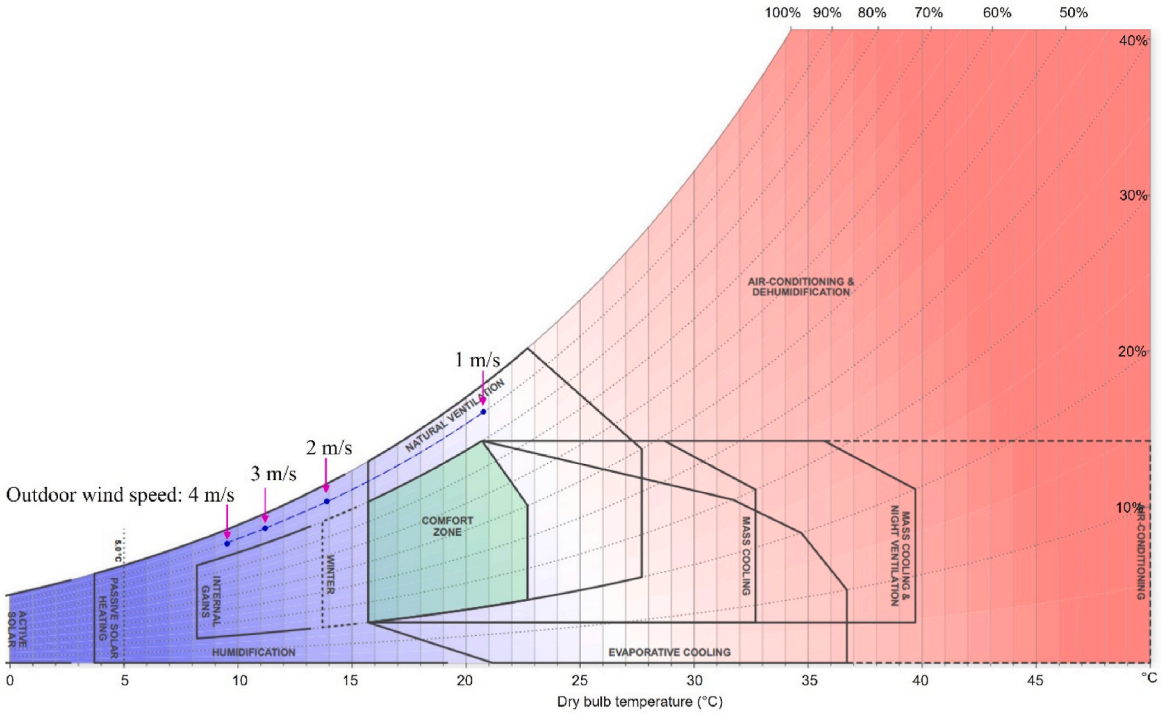

(a)

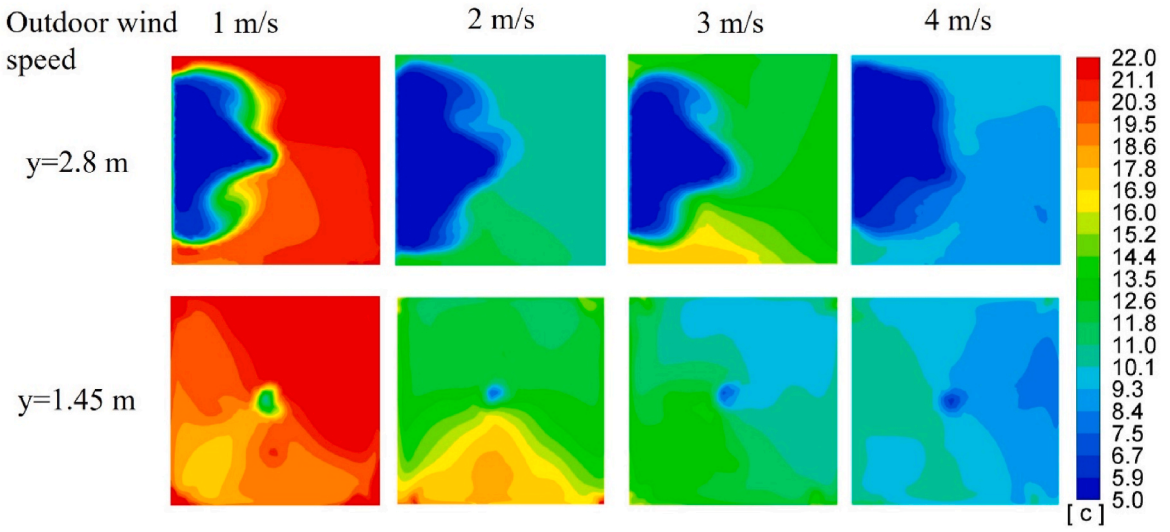

(b)

Fig. 17. (a) Psychrometric chart of the indoor temperatures and (b) the temperature contours at the heights of y = 1.45 m and 2.8 m at the wind speeds of 1–4 m/s.

ranging from 0.1 to 1.25 m/s and temperatures around −0.6 °C and 0.9 °C. The field experimental results indicate that relying on modelling work using static boundary conditions or conducting experiments in controlled environments such as wind tunnel testing to investigate the ventilation process is insufficient and may lead to inaccurate predictions, given that fluctuations or irregular patterns have been observed in the field experiments. Furthermore, a case study is conducted on a typical-sized primary school classroom occupied by 30 pupils and 1 teacher, using windcatcher ventilation. The outdoor temperature is fixed at 5 °C, wind speeds are 1–4 m/s with a wind angle of 0°, and a heat flux of 42 W/m^2 is evenly distributed on the classroom floor. The CFD simulation results indicate that the ventilation heat loss shows an increasing trend as the wind speeds increase. At the average yearly-round wind speed in the UK, which is typically above 2 m/s, there is a high chance that over-ventilation is occurring. A wind speed of 3 m/s can lead to an additional heat loss of 941.4 W due to over-ventilation. This corresponds to an extra heating load of 4.7 kWh and an additional heating electricity cost of £1.6 for a single classroom during a 5-h occupied period.

From the discussion, windcatcher ventilation alone might not be suitable for cold/mild-cold climates as it can cause thermal discomfort and significant ventilation heat loss. Windcatchers in cold climates must strike a balance between ventilation and thermal comfort, which is important for understanding its long-term cost-efficiency. Incorporating heat recovery devices, thermal energy storage systems, or adaptable control strategies into windcatchers may offer solutions to these

challenges. Further investigation could also explore the interactions between different heating systems and windcatcher ventilation. The numerical findings in this work may have limited validity for low-velocity flows and buoyancy-driven flows with significant temperature gradients. More advanced simulation tools, such as Large Eddy Simulation (LES), could potentially yield more accurate results in such cases. Conducting full-scale field experiments based on more realistic building scenarios is suggested to fully understand windcatchers' performance. Heat loss factors such as infiltration should be further considered. Solutions to prevent ASC or airflow disturbances among supply and exhaust quadrants should be implemented in future experiments, and local ventilation effectiveness in occupied spaces should be evaluated. Such insights are essential for developing more efficient and energy-conscious design strategies for ventilation in cold climates.

CRediT authorship contribution statement

Miaomiao Liu: Writing – review & editing, Writing – original draft, Visualization, Validation, Methodology, Investigation, Formal analysis, Data curation, Conceptualization. **Salah Almazmumi:** Methodology. **Pinlu Cao:** Writing – review & editing, Resources, Methodology. **Carlos Jimenez-bescos:** Supervision. **John Kaiser Calautit:** Writing – review & editing, Resources, Methodology.

Declaration of competing interest

The authors declare that they have no known competing financial interests or personal relationships that could have appeared to influence the work reported in this paper.

Data availability

Data will be made available on request.

Acknowledgements

The support by the China Scholarship Council and University of Nottingham is gratefully acknowledged.

Nomenclature

Abbreviation

CFD	Computational Fluid Dynamics
EAHE	Earth-air heat exchanger
ACH	Air changes per hour
ASC	Air short circuit
MAA	Mean age of air
ACE	Air change effectiveness
ABL	Atmospheric boundary layer
RANS	Reynolds-averaged Navier-Stokes
PMV	Predicted Mean Vote
RNG	Renormalization Group
LES	Large Eddy Simulation
UDS	user-defined scalar

Symbols

W	Width (m)
H	Height (m)
L	Length (m)
T	Temperature (K, °C)
t	Time
N	ACH (1/h)
v	Air velocity (m/s)
A	Area (m^2)
V	Volume of the test room (m^3)
Q	Ventilation heat loss (W)
q	Ventilation rate (L/s/m^2, L/s/person, m^3/s)
p	Pressure (Pa)
τ	Stress tensor (Pa)
ρ	Density (kg/m^3)
g	Gravitational acceleration (m/s^2)
F	External body force (N)
e	Internal energy (J)
h	Enthalpy (J)
κ	Thermal conductivity (W/m·K)
J	Diffusion flux (mol/m^2·s)
k	Turbulence kinetic energy (m^2/s^2)
ε	Dissipation rate (m^3/s^3)
G	Turbulence kinetic energy from mean velocity gradients or buoyancy (m^2/s^2)
Y	Compressible turbulence dissipation due to dilatation (J/m^3/s)
α	Prandtl number
S	User-defined source terms (kg/m3·s, J, m2/s2, m3/s3)
Φ	MAA (s)

λ	ACE
Γ	Diffusion coefficient
S_{ct}	Turbulent Schmidt number
y+	Distance of the first grid point away from the wall

Subscript

w	Windcatcher
r	Room
i	Indoor
o	Outdoor
c	Classroom
LE	Large
SL	Small
eff	Effective
f	Fluid
j	Species
b	Buoyancy
m	Mass
h	Heat
k	Turbulence kinetic energy
ε	Dissipation rate
s	Supply plane
n	Nominal
bh	Breathing height

Appendix

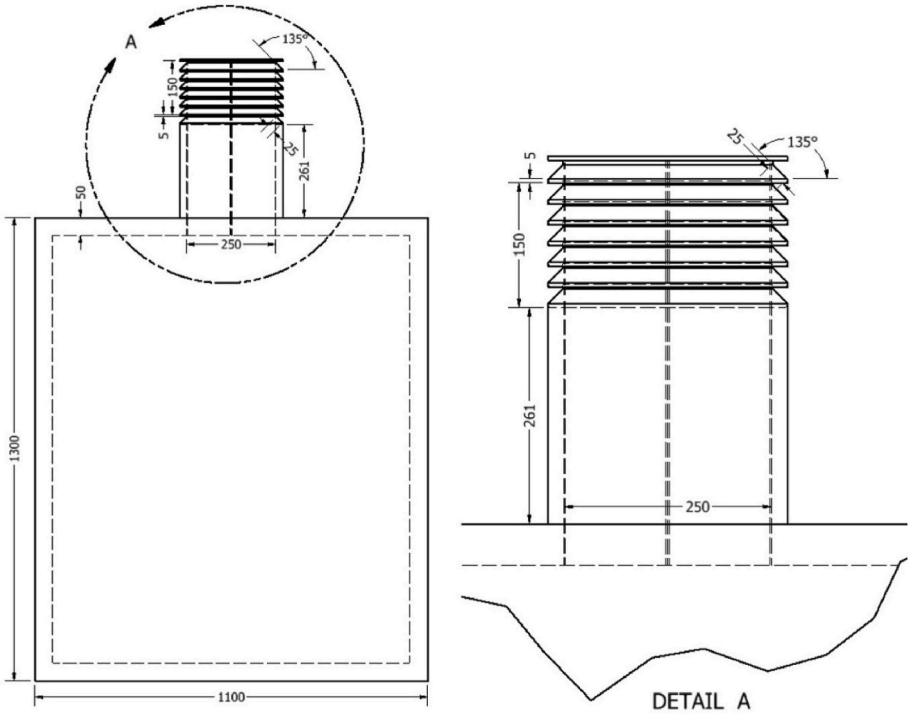

Fig. A.1. The dimensions of the windcatcher device and test room (units: mm).

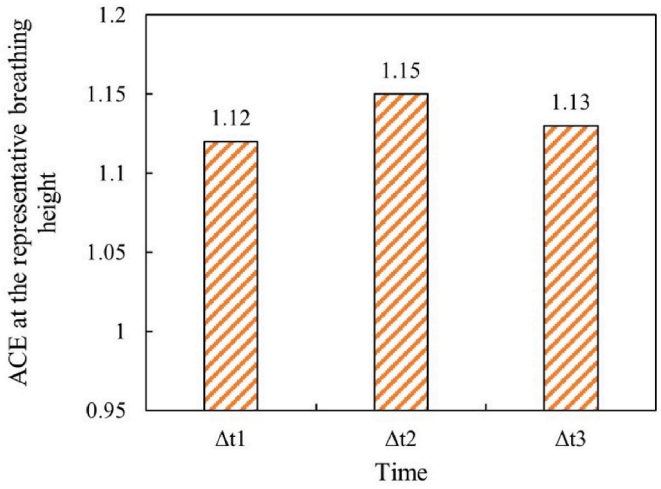

Fig. A.2. ACE values at the representative breathing height during Δt_1, Δt_2 and Δt_3.

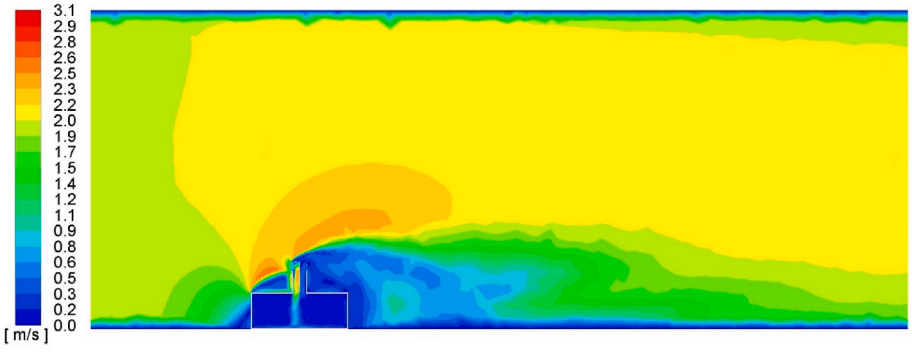

(a)

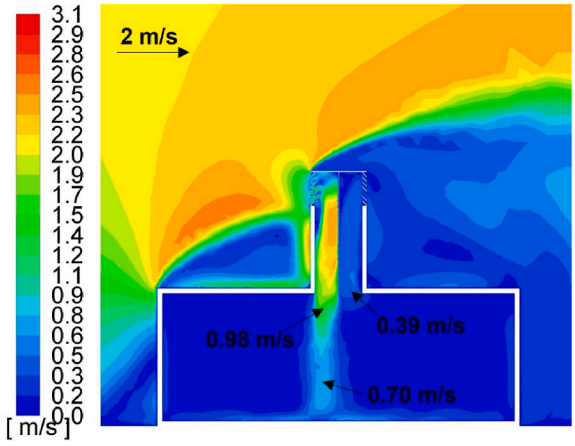

(b)

Fig. A.3. (a) The overall velocity distribution of the fluid domain and (b) the zoom-in view of the velocity distribution in the windcatcher and classroom.

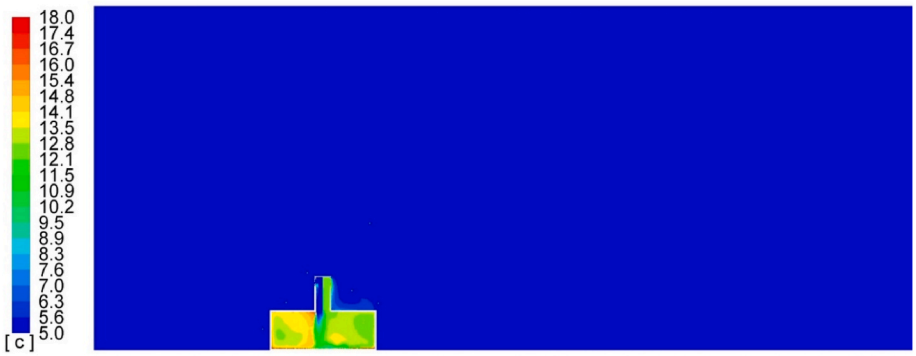

(a)

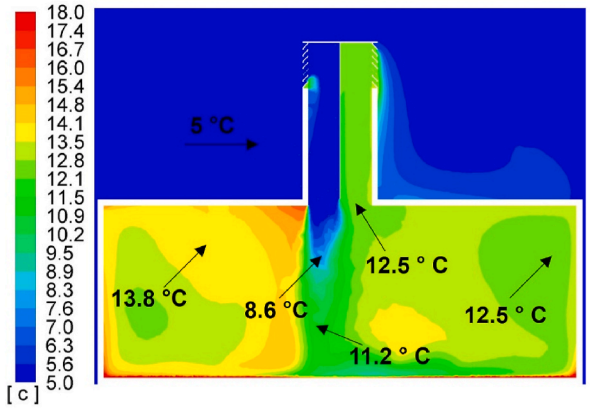

(b)

Fig. A.4. (a) The overall temperature distribution of the fluid domain and (b) the zoom-in view of the temperature distribution in the windcatcher and classroom. Air short circuit (ASC) can have significant effects on both nominal air change rates and the room air change rates in the breathing level. To further analyse the impact of air disturbances or ASC on indoor ventilation, the distribution of MAA and ACE in the windcatcher with and without the anti-ASC device was presented, as shown in Figs. A.5 and A.6. The design of the anti-ASC device followed the study by Nejat et al. [58]. In Fig. A.5, compared to the windcatcher with the anti-ASC device, higher MAA values were observed in the current work (without the anti-ASC device), especially below the representative occupants' breathing height. As shown in Fig. A.6, the average ACE in the current work was 1.03, whereas with the ASC device, the average ACE increased to 1.10. The recirculation zone area was decreased after including the anti-ASC device. These observations indicate that ASC may lead to lower local air change rates and decrease the overall ventilation effectiveness. Areas impacted by ASC could experience stagnant air, resulting in poor air quality and discomfort for occupants.

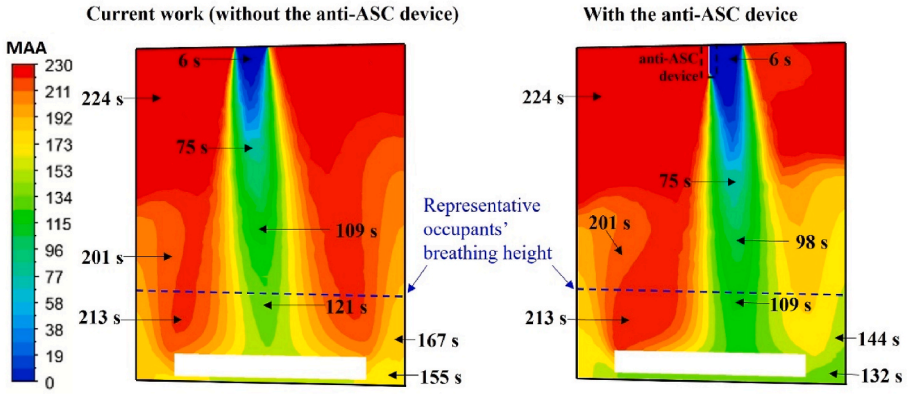

Fig. A.5. The MAA distribution on the cross-sectional plane with and without the anti-ASC device.

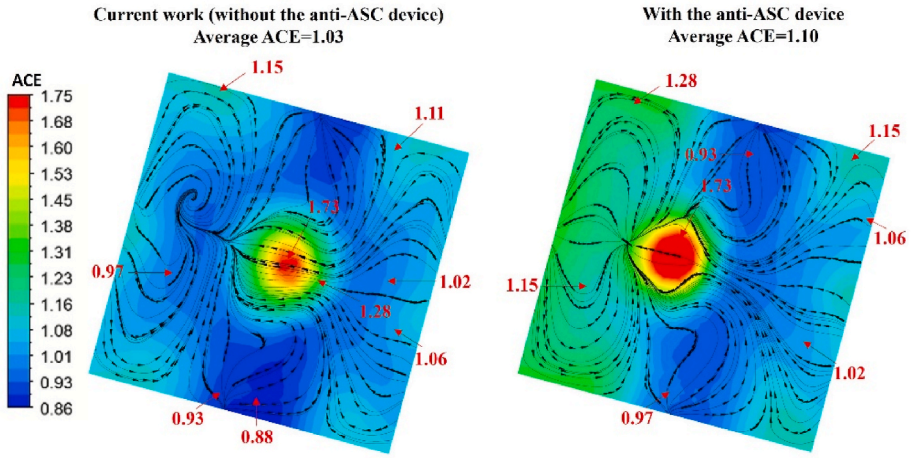

Fig. A.6. The ACE distribution and streamlines at the representative breathing height with and without the anti-ASC device.

References

[1] F. Jomehzadeh, et al., A review on windcatcher for passive cooling and natural ventilation in buildings, Part 1: indoor air quality and thermal comfort assessment, Renew. Sustain. Energy Rev. 70 (2017) 736–756.

[2] H. Montazeri, R. Azizian, Experimental study on natural ventilation performance of one-sided wind catcher, Build. Environ. 43 (12) (2008) 2193–2202, https://doi.org/10.1016/j.buildenv.2008.01.005.

[3] J. Foroozesh, et al., CFD modeling of the building integrated with a novel design of a one-sided wind-catcher with water spray: focus on thermal comfort, Sustain. Energy Technol. Assessments 53 (2022), 102736, https://doi.org/10.1016/j.seta.2022.102736.

[4] A.S.H. Abdallah, A new design of passive air condition integrated with solar chimney for hot arid region of Egypt, Int. J. Environ. Sci. Technol. 16 (2019) 2611–2618.

[5] J. Gao, A. Li, X. Xu, W. Gang, T. Yan, Ground heat exchangers: applications, technology integration and potentials for zero energy buildings, Renew. Energy 128 (2018) 337–349, https://doi.org/10.1016/j.renene.2018.05.089.

[6] J.K. Calautit, P.W. Tien, S. Wei, K. Calautit, B. Hughes, Numerical and experimental investigation of the indoor air quality and thermal comfort performance of a low energy cooling windcatcher with heat pipes and extended surfaces, Renew. Energy 145 (2020) 744–756, https://doi.org/10.1016/j.renene.2019.06.040.

[7] Z. Moghtader Gilvaei, et al., A novel passive system for providing natural ventilation and passive cooling: evaluating thermal comfort and building energy, Renew. Energy 198 (2022) 463–483, https://doi.org/10.1016/j.renene.2022.07.151.

[8] S. Jafari, V. Kalantar, Numerical simulation of natural ventilation with passive cooling by diagonal solar chimneys and windcatcher and water spray system in a hot and dry climate, Energy Build. 256 (2022), 111714, https://doi.org/10.1016/j.enbuild.2021.111714.

[9] H. Sadeghi, V. Kalantar, Performance analysis of a wind tower in combination with an underground channel, Sustain. Cities Soc. 37 (2018) 427–437.

[10] P. Abdo, B.P. Huynh, A. Braytee, R. Taghipour, An experimental investigation of the thermal effect due to discharging of phase change material in a room fitted with a windcatcher, Sustain. Cities Soc. 61 (2020), 102277.

[11] P. Nejat, M.S. Ferwati, J. Calautit, A. Ghahramani, M. Sheikhshahrokhdehkordi, Passive cooling and natural ventilation by the windcatcher (Badgir): an experimental and simulation study of indoor air quality, thermal comfort and passive cooling power, J. Build. Eng. 41 (2021), 102436.

[12] J.P. Harrouz, K. Ghali, N. Ghaddar, Integrated solar–Windcatcher with dew-point indirect evaporative cooler for classrooms, Appl. Therm. Eng. 188 (2021), 116654.

[13] M. Sadeghi, G. Wood, B. Samali, R. de Dear, Effects of urban context on the indoor thermal comfort performance of windcatchers in a residential setting, Energy Build. 219 (2020), 110010, https://doi.org/10.1016/j.enbuild.2020.110010.

[14] P.V. Dorizas, et al., Performance of a natural ventilation system with heat recovery in UK classrooms: an experimental study, Energy Build. 179 (2018) 278–291, https://doi.org/10.1016/j.enbuild.2018.09.005.

[15] E. Cuce, F. Sher, H. Sadiq, P.M. Cuce, T. Guclu, A.B. Besir, Sustainable ventilation strategies in buildings: CFD research, Sustain. Energy Technol. Assessments 36 (Dec) (2019), https://doi.org/10.1016/j.seta.2019.100540.

[16] D. O'Connor, J.K. Calautit, B.R. Hughes, D. O'Connor, J.K. Calautit, B.R. Hughes, A study of passive ventilation integrated with heat recovery, Energy Build. 82 (Oct. 2014) 799–811, https://doi.org/10.1016/j.enbuild.2014.05.050.

[17] J.K. Calautit, D. O'Connor, B.R. Hughes, A natural ventilation wind tower with heat pipe heat recovery for cold climates, Renew. Energy 87 (2016) 1088–1104, https://doi.org/10.1016/j.renene.2015.08.026.

[18] J.K. Calautit, D. O'Connor, P.W. Tien, S. Wei, C.A.J. Pantua, B. Hughes, Development of a natural ventilation windcatcher with passive heat recovery wheel for mild-cold climates: CFD and experimental analysis, Renew. Energy 160 (2020) 465–482, https://doi.org/10.1016/j.renene.2020.05.177.

[19] H. Mahon, D. Friedrich, B. Hughes, Wind tunnel test and numerical study of a multi-sided wind tower with horizontal heat pipes, Energy 260 (2022), 125118.

[20] M. Liu, C. Jimenez-Bescos, J. Calautit, CFD investigation of a natural ventilation wind tower system with solid tube banks heat recovery for mild-cold climate, J. Build. Eng. 45 (2022), 103570, https://doi.org/10.1016/j.jobe.2021.103570.

[21] M. Liu, C. Jimenez-Bescos, J.K. Calautit, Performance evaluation of wind tower natural ventilation with passive solid tube heat recovery based on CO2 levels, J. Build. Eng. 72 (2023), 106457.

[22] J.K. Calautit, B.R. Hughes, D.S.N.M. Nasir, Climatic analysis of a passive cooling technology for the built environment in hot countries, Appl. Energy 186 (2017) 321–335, https://doi.org/10.1016/j.apenergy.2016.05.096.

[23] M. Liu, C. Jimenez-Bescos, J.K. Calautit, Passive heat recovery wind tower: assessing the overheating risk in summertime and ventilation heat loss reduction in wintertime, Sustain. Energy Technol. Assessments 58 (2023), 103310.

[24] ANSYS FLUENT 12.0 User's guide [Online]. Available: https://www.afs.enea.it/project/neptunius/docs/fluent/html/th/node11.htm. (Accessed 16 June 2023).

[25] S. Liu, C.M. Mak, J. Niu, Numerical evaluation of louver configuration and ventilation strategies for the windcatcher system, Build. Environ. 46 (8) (2011) 1600–1616, https://doi.org/10.1016/j.buildenv.2011.01.025.

[26] J.A. Castillo, G. Huelsz, T. van Hooff, B. Blocken, Natural ventilation of an isolated generic building with a windward window and different windexchangers: CFD validation, sensitivity study and performance analysis, in: Building Simulation, Springer, 2019, pp. 475–488.

[27] Y. Wu, N. Gao, J. Niu, J. Zang, Q. Cao, Numerical study on natural ventilation of the wind tower: effects of combining with different window configurations in a low-rise house, Build. Environ. 188 (2021), 107450.

[28] M.K. Esfeh, A. Sohankar, A.R. Shahsavari, M.R. Rastan, M. Ghodrat, M. Nili, Experimental and numerical evaluation of wind-driven natural ventilation of a curved roof for various wind angles, Build. Environ. 205 (2021), 108275.

[29] N. Nasrollahi, P. Ghobadi, Field measurement and numerical investigation of natural cross-ventilation in high-rise buildings; Thermal comfort analysis, Appl. Therm. Eng. 211 (2022), 118500.

[30] S.H. Hosseini, E. Shokry, A.J. Ahmadian Hosseini, G. Ahmadi, J.K. Calautit, Evaluation of Airflow and Thermal Comfort in Buildings Ventilated with Wind Catchers: Simulation of Conditions in Yazd City, Iran, vol. 35, Energy for Sustainable Development, 2016, pp. 7–24, https://doi.org/10.1016/j.esd.2016.09.005.

[31] A. Rezaeiha, H. Montazeri, B. Blocken, On the accuracy of turbulence models for CFD simulations of vertical axis wind turbines, Energy 180 (2019) 838–857.

[32] N. Serra, Revisiting RANS turbulence modelling used in built-environment CFD simulations, Build. Environ. 237 (2023), 110333.

[33] Monodraught Ltd., Cranbrook primary school, windcatchers [Online]. Available: https://www.monodraught.com/projects/cranbrook-primary-school. (Accessed 11 August 2023).

[34] Monodraught Ltd., Tranent North primary school, windcatchers [Online]. Available: https://www.monodraught.com/projects/tranent-north-primary-school. (Accessed 11 August 2023).

[35] U. Department for Education, Building Bulletin 103: area guidelines for mainstream schools [Online]. Available: https://assets.publishing.service.gov.uk/government/uploads/system/uploads/attachment_data/file/905692/BB103_Area_Guidelines_for_Mainstream_Schools.pdf. (Accessed 10 June 2023).

[36] Building Bulletin 103: area guidelines for mainstream schools [Online]. Available: https://assets.publishing.service.gov.uk/government/uploads/system/uploa

ds/attachment_data/file/905692/BB103_Area_Guidelines_for_Mainstream_Schools.pdf. (Accessed 8 June 2023).
[37] J. Franke, A. Hellsten, K.H. Schlunzen, B. Carissimo, The COST 732 Best Practice Guideline for CFD simulation of flows in the urban environment: a summary, Int. J. Environ. Pollut. 44 (1–4) (2011) 419–427.
[38] Y. Abu-Zidan, P. Mendis, T. Gunawardena, Optimising the computational domain size in CFD simulations of tall buildings, Heliyon 7 (4) (2021), e06723.
[39] A. Persily, L. de Jonge, Carbon dioxide generation rates for building occupants, Indoor Air 27 (5) (2017) 868–879.
[40] D. Wang, W. Li, Y. Liu, Y. Chen, L. Hu, H. Du, Non-uniform operative temperature distribution characteristics and heat-source-controlled core-area range of local heating radiators, in: Building Simulation, Springer, 2023, pp. 87–103.
[41] M. Lain, V. Zmrhal, J.L.M. Hensen, Low energy cooling of buildings in central Europe-case studies, Int. J. Vent. 7 (1) (2008) 11–21.
[42] J.K. Calautit, B.R. Hughes, Measurement and prediction of the indoor airflow in a room ventilated with a commercial wind tower, Energy Build. 84 (2014) 367–377, https://doi.org/10.1016/j.enbuild.2014.08.015.
[43] nw3 weather [Online]. Available: http://nw3weather.co.uk/charts.php?unit=UK. (Accessed 8 June 2023).
[44] R. Ramponi, B. Blocken, CFD simulation of cross-ventilation for a generic isolated building: impact of computational parameters, Build. Environ. 53 (2012) 34–48.
[45] J.K. Calautit, D. O'Connor, B.R. Hughes, A natural ventilation wind tower with heat pipe heat recovery for cold climates, Renew. Energy 87 (2016) 1088–1104.
[46] C.F. Gao, W.L. Lee, Evaluating the influence of openings configuration on natural ventilation performance of residential units in Hong Kong, Build. Environ. 46 (4) (2011) 961–969.
[47] M. V Swami, S. Chandra, Procedures for Calculating Natural Ventilation Airflow Rates in Buildings, 1987.
[48] N. Khammayom, N. Maruyama, C. Chaichana, M. Hirota, Impact of environmental factors on energy balance of greenhouse for strawberry cultivation, Case Stud. Therm. Eng. 33 (2022), 101945.
[49] F. Hall, Building Services and Equipment, third ed., vol. 1, Routledge, 1994.
[50] R. Ramponi, B. Blocken, L.B. de Coo, W.D. Janssen, CFD simulation of outdoor ventilation of generic urban configurations with different urban densities and equal and unequal street widths, Build. Environ. 92 (2015) 152–166.
[51] Z. Cao, Y. Wang, C. Zhai, M. Wang, Performance evaluation of different air distribution systems for removal of concentrated emission contaminants by using vortex flow ventilation system, Build. Environ. 142 (2018) 211–220.
[52] V. Chanteloup, P.-S. Mirade, Computational fluid dynamics (CFD) modelling of local mean age of air distribution in forced-ventilation food plants, J. Food Eng. 90 (1) (2009) 90–103.
[53] P. Raphe, H. Fellouah, S. Poncet, M. Ameur, Ventilation effectiveness of uniform and non-uniform perforated duct diffusers at office room, Build. Environ. 204 (2021), 108118.
[54] E. Mundt, H.M. Mathisen, P. V Nielsen, A. Moser, Ventilation Effectiveness, Rehva, 2004.
[55] A. ASHRAE, "ASHRAE 129-1997 (RA 2002), Measuring Air Change Effectiveness, American Society of Heating, Refrigerating and Air-Conditioning Engineers, 2002.
[56] J.K. Calautit, B.R. Hughes, H.N. Chaudhry, S.A. Ghani, CFD analysis of a heat transfer device integrated wind tower system for hot and dry climate, Appl. Energy 112 (SI) (Dec. 2013) 576–591, https://doi.org/10.1016/j.apenergy.2013.01.021.
[57] [Online]. Available:, BB 101: Ventilation, Thermal Comfort and Indoor Air Quality, 2018 https://www.gov.uk/government/publications/building-bulletin-101-ventilation-for-school-buildings. (Accessed 6 June 2023).
[58] P. Nejat, J.K. Calautit, M. Z. Abd Majid, B.R. Hughes, F. Jomehzadeh, Anti-short-circuit device: a new solution for short-circuiting in windcatcher and improvement of natural ventilation performance, Build. Environ. 105 (2016) 24–39, https://doi.org/10.1016/j.buildenv.2016.05.023.
[59] Met office, UK climate averages [Online]. Available: https://www.metoffice.gov.uk/research/climate/maps-and-data/uk-climate-averages/gcpsvg3nc. (Accessed 11 August 2023).
[60] Energy Guide Uk, Average cost of electricity per KWh (UK 2023 updated) [Online]. Available: https://energyguide.org.uk/average-cost-electricity-kwh-uk/. (Accessed 10 June 2023).
[61] B. Givoni, Comfort, climate analysis and building design guidelines, Energy Build. 18 (1) (1992) 11–23.
[62] A. Lenoir, G. Baird, F. Garde, Post-occupancy evaluation and experimental feedback of a net zero-energy building in a tropical climate, Architect. Sci. Rev. 55 (3) (2012) 156–168.
[63] S. Attia, S. Carlucci, Impact of different thermal comfort models on zero energy residential buildings in hot climate, Energy Build. 102 (2015) 117–128.
[64] M.H. Khan, W. Pao, Thermal comfort analysis of PMV model prediction in air conditioned and naturally ventilated buildings, Energy Proc. 75 (2015) 1373–1379.
[65] D. N. C. Comite'Europe'en, EN 15251: indoor environmental input parameters for design and assessment of energy performance of buildings—addressing indoor air quality, thermal environment, lighting and acoustics [Online]. Available: http://www.cres.gr/greenbuilding/PDF/prend/set4/WI_31_Pre-FV_version_prEN_15251_Indoor_Environment.pdf. (Accessed 7 June 2023).
[66] G. Havenith, Metabolic rate and clothing insulation data of children and adolescents during various school activities, Ergonomics 50 (10) (2007) 1689–1701.
[67] D. O'Connor, J. Calautit, B.R. Hughes, Effect of rotation speed of a rotary thermal wheel on ventilation supply rates of wind tower system, Energy Proc. 75 (2015) 1705–1710, https://doi.org/10.1016/j.egypro.2015.07.432.